Fermi National Accelerator Laboratory

FERMILAB-Pub-324-A
September 1994

Light mesons production at the Tevatron to next-to-leading order

Mario Greco[a] and Simona Rolli[b] [1]

[a] *Dipartimento di Fisica, Università dell'Aquila, Italy*
INFN, Laboratori Nazionali di Frascati, Frascati, Italy

[b] *Dipartimento di Fisica Nucleare e Teorica,, Università di Pavia, Italy*
INFN, Sezione di Pavia, Pavia, Italy and
NASA/Fermilab Astrophysics Center, FERMILAB, Batavia, Il 60510

Abstract

Inclusive production of light mesons (π^0, η, $\pi^\pm$, $K^\pm$) at the Tevatron is considered in QCD to next-to-leading order in the formalism of fragmentation functions. We present various distributions of phenomenological interest, along with a new set of K mesons fragmentation functions.

[1] e-mail address:greco@lnf.infn.it, rolli@fnalv.fnal.gov

Operated by Universities Research Association Inc. under contract with the United States Department of Energy

The study of inclusive particle production in hadron-hadron collisions is interesting for giving information on the fragmentation properties of partons in perturbative QCD and the hadronization mechanisms. From the theoretical point of view this means that one has to know separately parton distribution functions, partonic cross sections and fragmentation functions: the factorization theorem in fact insures that the inclusive cross section can be written as a convolution of these different terms. While different sets of parton distribution functions do exist at next-to-leading order(NLO) [1], and also partonic cross sections have been evaluated to one-loop accuracy [2], for the fragmentation functions (FF) we are only at the beginning, only a few sets existing at NLO accuracy [3, 4, 5, 6, 7]. Indeed the study of calorimetric jet cross sections has been of primary interest during last few years, and only now experiments are providing us information on inclusive production of single hadrons.

In previous analyses [3, 4, 5] FF have been evaluated at next-to-leading order for neutral and charged pions, and for the eta meson, using two different methods. In the first approach, one starts with a very simple parametrization of the parton FF at $Q_0^2 \sim$ few GeV^2, and fits $e+e-$ data after NLO evolution. Alternatively, a Montecarlo simulator is used to parametrize the parton FF at $Q_0^2 \sim 30$ GeV^2 and, again after NLO evolution, e^+e^- data are well reproduced. Both methods are in good agreement, and indeed with these sets we were able to reproduce data obtained in hadron collisions in fixed target experiments and at the Cern $Sp\bar{p}S$ collider.

In this Letter we present a new set of FF for charged and neutral kaons, along with various distributions of phenomenological interest regarding the production of light mesons at high p_t, for $\sqrt{s} = 1800$ GeV, due to the lack of NLO predictions at these energies. Indeed in a previous work Borzumati et al. [9] have given some predictions on inclusive hadron production at Tevatron, but in a low p_t range and using obsolete LO sets of fragmentation functions [10].

We would like to remind that the study of neutral clusters production could be useful in the evaluation of background to a possible Higgs signal. On the other hand inclusive particle production will help in understanding the jet fragmentation properties in QCD

In the following we will first briefly discuss the theoretical framework for calculating the single inclusive particle cross section in hadron-hadron collisions, and then we will present and discuss various phenomenological results.

We report, for reader's convenience, the main formulae for one hadron inclusive production at next-to-leading-order, via the reaction $A + B \to H + X$, where A and B are incoming hadrons. The cross section is given by the convolution of the partonic cross section and the fragmentation functions $D_l^H(z, M_f^2)$:

$$E_H \frac{d\sigma_{A+B\to H}}{d^3\vec{P}_H} = \sum_l \int_{z_H}^1 \frac{dz}{z^2} D_l^H(z, M_f^2)\, E_l \frac{d\sigma_{A+B\to l}}{d^3\vec{P}_l}(\frac{z_H}{z}, \theta, \alpha_s(\mu^2), M_f^2, \cdots), \tag{1}$$

where z_H is the reduced energy of the hadron H, $z_H = 2E_H/\sqrt{S}$, θ is the scattered angle of the parton l, and the inclusive production of the parton l in the reaction $A + B \to l$ has the following perturbative development:

$$E_l \frac{d\sigma_{A+B\to l}}{d^3\vec{P}_l}(\frac{z_H}{z}, \theta, \alpha_s(\mu^2), M_f^2, \cdots) = \sigma^0_{A+B\to l}(\frac{z_H}{z}, \theta) + \frac{\alpha_s(\mu^2)}{2\pi}\, \sigma^1_{A+B\to l}(\frac{z_H}{z}, \theta, M_f^2) + \cdots. \tag{2}$$

$D_l^H(z, M_f^2)$ represents the number of hadrons H inside the parton l carrying the fraction of momentum z from H, evolved at the scale M_f^2. These fragmentation functions satisfy the usual Altarelli-Parisi type evolution equations .

The partonic cross-sections are [2, 3]:

$$\begin{aligned} E_l \frac{d\sigma_{p+p\to l}}{d^3\vec{P}_l}(y, \theta, \alpha_s(\mu^2), M_f^2) &= \frac{1}{\pi S} \sum_{i,j} \int_{VW}^{V} \frac{dv}{1-v} \int_{VW/v}^{1} \frac{dw}{w} \\ &\times \left[F_i^p(x_1, M^2) F_j^p(x_2, M^2) \left(\frac{1}{v} \left(\frac{d\sigma^0}{dv} \right)_{ij\to l} (s, v)\delta(1-w) \right.\right. \\ &\left.\left. + \frac{\alpha_s(\mu^2)}{2\pi} K_{ij\to l}(s, v, w; \mu^2; M^2, M_f^2) \right) + (x_1 \leftrightarrow x_2) \right], \end{aligned} \tag{3}$$

where the partonic variables are $s = x_1 x_2 S$ and

$$x_1 = \frac{VW}{vw}, \quad x_2 = \frac{1-V}{1-v},$$

and the hadronic ones are defined by:

$$V = 1 - \frac{y}{2}(1 - \cos\theta), \quad W = \frac{y(1+\cos\theta)}{2 - y(1-\cos\theta)}.$$

In the partonic cross sections to one loop [2], calculated from the squared matrix elements $O(\alpha_S^3)$ of Ellis et Sexton [11], the initial state collinear divergences have been factorised and absorbed into the dressed structure functions in the $\overline{MS}$ scheme. Coherently with this choice, we have used for the proton structure functions set B1 of Morfin & Tung, [12] (set A), set MRS D0 of Martins Roberts & Stirling [13] (set B), and set GRV HO of Glück, Reya & Vogt [14] (set C).

We have used α_s calculated at 2-loop, with 5 flavours and with $\Lambda_{QCD} = 200\ MeV$. Set A of nucleon structure functions has been indeed evolved with $\Lambda_{QCD} = 194\ MeV$.

As already stated above, FF will be considerd to NLO accuracy. For the π^0 case, various consistent parametrizations have been discussed in ref. [3], using different methods and initial conditions. All of them have been successfully compared with the current experimental data in e^+e^- and $p\bar{p}$ collisions at various energies. In the following we will use only one set of them [5], based on the latter version of the MonteCarlo simulator HERWIG [15, 16], which is used to fix the initial conditions at the fragmentation scale $M_0 = 30$ GeV. The same method has also been applied in ref.[4] to inclusive η production, and indeed the predicted η/π^0 ratio has been found to agree with the present experimental information at ISR [17] and from e^+e^- and $p\bar{p}$ colliders. Recent fixed target experiments also agree [18] with the predictions of ref. [4], and further constrain the gluon FF for η. In reference [5] we have adopted the same technique to extract the charged pion FF, in good agreement with the neutral pion set assuming $SU(2)$ symmetry.

We are therefore quite confident of the reliability of the method and consequently we use the same tecnique to obtain a new set of FF for charged kaons and K^0_s: they are very similar in slope (with the appropriate interchanges between u, $\bar{u}$ and d, $\bar{d}$), differing only by a normalization factor, as we expect. So we will present final results for for the production cross sections for charged kaons only.

As usual the functions are parametrized as:

$$D^h_i(z, M_0^2) = N_i z^{\alpha_i}(1-z)^{\beta_i} \tag{4}$$

where i runs over (u, d, s, c, b, g), and $M_0 = 30$ GeV. The coefficients are given in Table I and II (we indicate the average multiplicity of produced hadrons with the symbol $< n_i >$).

We now present various numerical results, starting, in Fig.1, with the p_t distribution for inclusive single particle production for π^0, η, $\pi^\pm$, $K^\pm$, integrated in the region of pseudorapidity $\eta = -\ln(\tan(\frac{\theta}{2}))$ between -0.7 and 0.7 and using the Set B-1 of Morfin and Tung [12]. We set all the scales equal to the p_T of the produced hadron.

In Figs. 2 we study the dependence on factorization, fragmentation and normalization scales. We vary the scales simultaneusly for different values of p_t and obtain that the cross sections change of about 20% for $0.5 < \xi < 2$, the variation being reduced at high p_T. This is explicitly shown in Figs. 3, where we plot the p_t distributions for different choices of the scale ($\xi = M/p_t$=0.5, 1, 2).

In Figs. 4 we present the η distributions for π^0 and $\pi^\pm$ production for different values of p_t in the region $|\eta| \leq 2$.

In Figs. 5 we show the contributions from different subprocesses, i.e. qq, qg and

gg, where q refers to the sum of q and $\bar{q}$ in the initial state, for $\eta = 0$ and using Set B1 of Morfin and Tung. In order to study the sensitivity to different parton distributions we plot in Figs. 6 the ratio of the cross sections for the subprocess $gg \to h + X$ for two other sets of proton structure functions, i.e. MRS-D0, GRV-HO, with respect to the set MT-B1. The variations are confined within about 10%. The sum over all parton subprocesses generally reduces the effect, as shown in Figs. 7, with the exception of the GRV-HO set for kaons production.

In order to disentangle the fragmentation properties and the hadronization mechanism of high p_t jets, we consider next the ratio between the single hadron and jet cross sections, for fixed values of the variable $z = E_{hadr}/E_{jet}$. Then, using the jet algorithm of ref.[19, 20] and the NLO evaluation of the jet cross sections of ref. [2], we present in Fig.8 a preliminary result[8] on jet fragmentation in charged and neutral pions, with the energy of the jet varying between 40 and 70 GeV, with a jet cone radius R=0.7 centered around the $\eta = 0$ direction. The overall theoretical uncertainty -which is not reported in figure- can be estimated to be of order 50%. We also show the analogous experimental result on jet fragmentation in charged hadrons[22], in reasonable agreement with the theoretical prediction.

As a final result we give a mean value for the ratio R=$\eta/\pi^0 = 1.15 \pm .30$, in the range 20 Gev $< p_t <$ 200 GeV which agrees with the recent experimental value of R=$1.02 \pm 0.15 \pm 0.23$ [21]. The theoretical uncertainty is related to the variation of the scales in parton distributions and fragmentation functions.

To conclude, we have presented various theoretical results of phenomenological interest at the Tevatron, concerning the inclusive production of light mesons in QCD to NLO. We have studied the uncertainty with respect to the choice of the scales and different sets of proton structure functions. We have also presented new sets of fragmentation functions for neutral and charged kaons.

One of us (S.R.) would like to aknowledge Joey Huston and Rob Blair of CDF Collaboration for useful discussions, and Andrea Parri of CDF and KLOE collaborations for precious suggestions about graphics.

This work was supported in part by the DOE and by the NASA (NAGW-2831) at Fermilab.

Table Captions

- Table I: parameters of the $K^{\pm}$ fragmentation functions at $M_0 = 30$ GeV (see eq.4).
- Table II: parameters of the K_s^0 fragmentation functions at $M_0 = 30$ GeV (see eq.4).

Figure Captions

- Fig. 1: P_t distribution for π^0, η, $\pi^{\pm}$, $K^{\pm}$ production, at $\sqrt{s} = 1800$ GeV and $|\eta| \leq 0.7$.
- Figs. 2: π^0, η, $\pi^{\pm}$, $K^{\pm}$ production, $\sqrt{s} = 1800$ GeV. Dependence of $\frac{d\sigma}{dp_t}$ on the renormalization, factorization and fragmentation mass scales: $\mu = M_p = M_f = \xi p_t$ for $p_t = 20,\ 80,\ 160,\ 200$ GeV and $|\eta| \leq 0.7$.
- Figs. 3: P_t distribution for π^0, η, $\pi^{\pm}$, $K^{\pm}$ production, $\sqrt{s} = 1800$ GeV . for different values of $\xi = M/p_t$, and using Set B1 of Morfin & Tung.
- Figs. 4: π^0, $\pi^{\pm}$ production. η distributions of $\frac{d\sigma}{d\eta dp_t}$ at fixed p_t.
- Figs. 5: π^0, η, $\pi^{\pm}$, $K^{\pm}$ production, $\sqrt{s} = 1800$ GeV. $\frac{d\sigma}{d\eta dp_t}$, for various partonic subprocesses (q refers to the sum of q and $\bar{q}$ in the initial state).
- Figs. 6: π^0, η, $\pi^{\pm}$, $K^{\pm}$ production, $\sqrt{s} = 1800$ GeV. p_t distribution at $\eta = 0$, for the subprocess $gg \to \pi^0 + X$ for different sets of proton structure functions. Curves are normalized to the MT-B1 set of proton structure functions.
- Figs. 7:π^0, η, $\pi^{\pm}$, $K^{\pm}$ production, $\sqrt{s} = 1800$ GeV. Dependence of $\frac{d\sigma}{d\eta dp_t}$ on different sets of parton distributions. Curves are normalized to the set MT-B1 of proton structure functions.
- Fig.8: jet fragmentation function, into π^0 and $(\pi^+ + \pi^-)$. Ratio of the inclusive hadron cross section to the inclusive jet cross section for $h = \pi^0$ and $(\pi^+ + \pi^-)$, as function of $z = E_h/E_{jet}$. The experimental points refer to charged hadrons and are from reference [22].

Parton	α	β	N_i	$< n_i >$
u	-1.42 ± 0.03	1.48 ± 0.13	0.1	0.59
d	-1.10 ± 0.03	4.32 ± 0.05	0.34	0.55
s	-0.83 ± 0.03	1.13 ± 0.03	0.57	0.95
c	-0.70 ± 0.03	3.78 ± 0.08	1.41	1.01
b	-0.77 ± 0.03	7.7 ± 0.18	2.82	1.24
g	-0.39 ± 0.03	4.74 ± 0.08	1.97	0.62

Table I

Parton	α	β	N_i	$< n_i >$
u	-1.06 ± 0.03	4.37 ± 0.13	0.19	0.27
d	-1.39 ± 0.03	1.46 ± 0.05	0.05	0.28
s	-0.84 ± 0.03	1.01 ± 0.03	0.26	0.45
c	-0.80 ± 0.03	3.31 ± 0.08	0.50	0.49
b	-0.63 ± 0.03	8.15 ± 0.18	2.02	0.62
g	-0.56 ± 0.03	4.26 ± 0.08	0.61	0.30

Table II

References

[1] See for example H. Plothow-Besch; Computer Physics Comm. 75 (1993) 396.

[2] F.Aversa, P.Chiappetta, M.Greco and J.Ph.Guillet; Nucl.Phys.B327 (1989) 105.

[3] P. Chiappetta, M. Greco, J. Ph. Guillet, S. Rolli and M. Werlen; Nucl. Phys. B 412 (1994) 3.

[4] M. Greco and S. Rolli; Z.Phys. C 60 (1993) 169.

[5] M. Greco , S. Rolli and A. Vicini; Fermilab-Pub-94/075-A and DFPD 94/TH/21

[6] J. Binnewies, B. A. Kniehl and G. Kramer; Desy 94-124

[7] Aleph Collaboration; Contribution to the 27th International Conference on High Energy Physics, Glasgow, Scotland. 20-27 July 1994

[8] Work in progress.

[9] F.M.Borzumati, B.A. Kniehl and G Kramer; Z.Phys. C 57 (1993) 595

[10] R. Baier, J. Engles and B. Petersson; Z. Phys. C 2 (1979) 265; M. Anselmino, P. Kroll and E. Leader; Z. Phys. C 18 (1983) 307.

[11] R.K.Ellis and J.C.Sexton; Nucl.Phys.B 269 (1986) 445.

[12] J.G.Morfin and Wu-Ki Tung; Z.Phys. C 52 (1991) 13.

[13] A. D. Martin, R. G. Roberts and W. J. Stirling; Phys. Rev. D 47 (1993) 867.

[14] M. Glück, E. Reya and A. Vogt; Z.Phys. C 53 (1992) 127

[15] G. Marchesini, B.R. Webber; Nucl Phys. B 238 (1984) 1.

[16] G. Marchesini, B.R. Webber; Nucl Phys. B 310(1988) 461.

[17] F. Büsser et al.; Nucl. Phys. B 106 (1976) 1.

[18] E706 Collaboration; talk given at Moriond 94.

[19] S.D. Ellis, Z. Kunszt and D.E Soper; Phys.Rev D40 (1989) 2188.

[20] J.E.Huth et al., Fermilab-Conf-90/249-E (1990).

[21] CDF Collaboration, Phys. Rev D (1993) 2998.

[22] CDF Collaboration, Phys. Rev. Lett. (1990) 968.

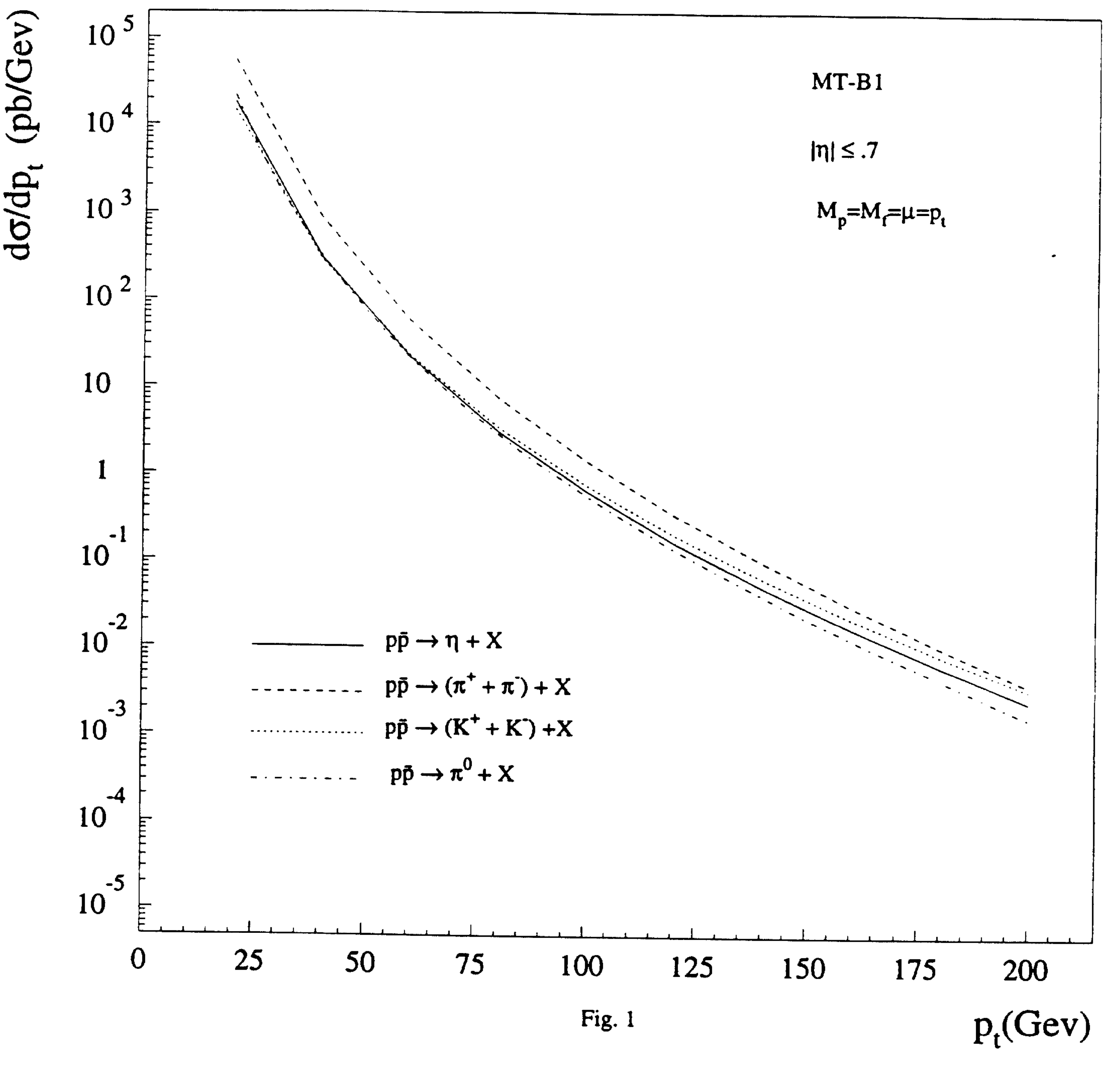

$d\sigma/dp_t$ (pb/Gev)
MT-B1
$|\eta| \le .7$
$M_p=M_f=\mu=p_t$
$p\bar{p} \to \eta + X$
$p\bar{p} \to (\pi^+ + \pi^-) + X$
$p\bar{p} \to (K^+ + K^-) + X$
$p\bar{p} \to \pi^0 + X$
p_t(Gev)

Fig. 1

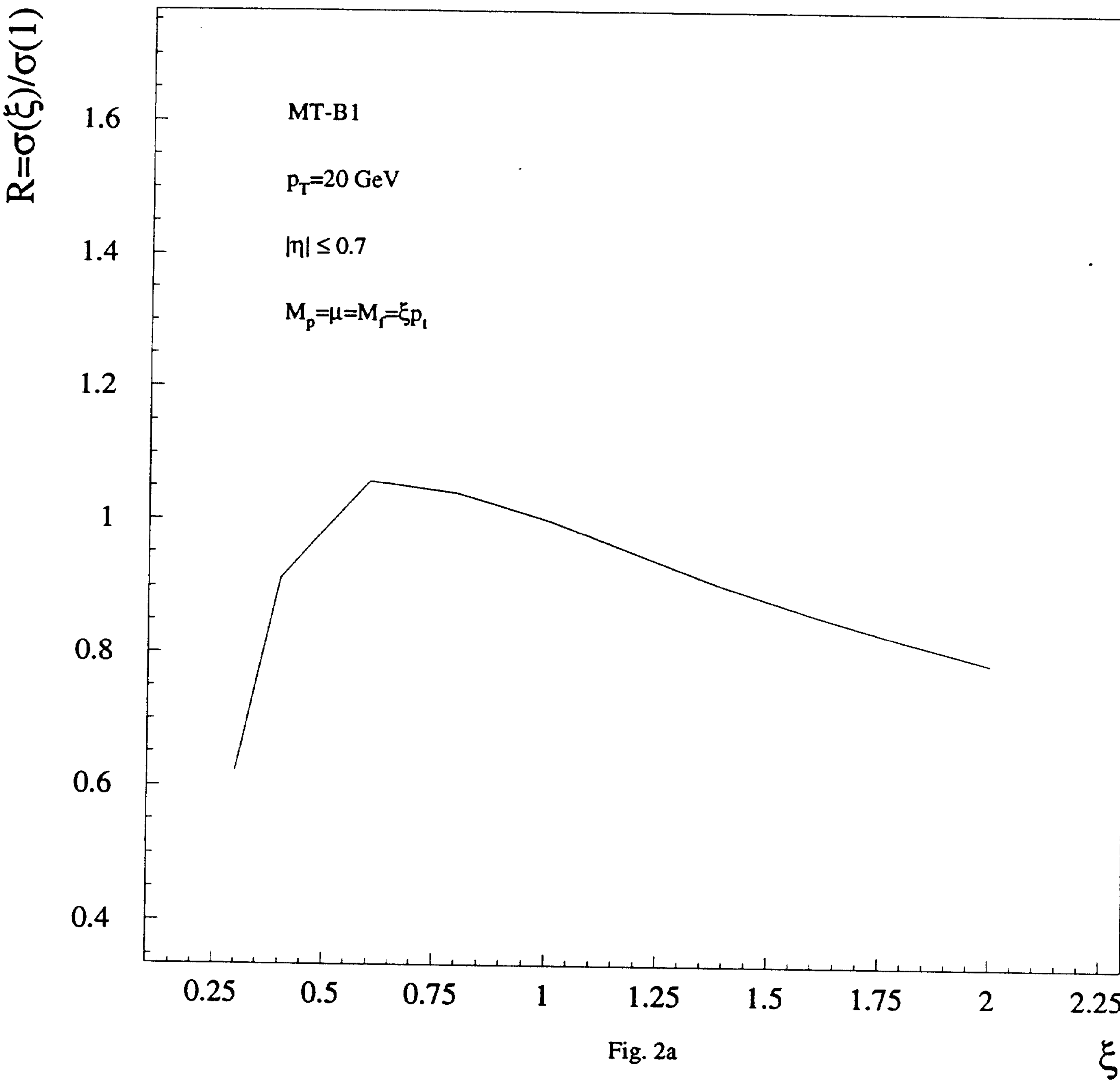
R=σ(ξ)/σ(1)
MT-B1
p_T=20 GeV
$|\eta| \leq 0.7$
$M_p=\mu=M_f=\xi p_t$
1.6
1.4
1.2
1
0.8
0.6
0.4
0.25
0.5
0.75
1
1.25
1.5
1.75
2
2.25
ξ

Fig. 2a

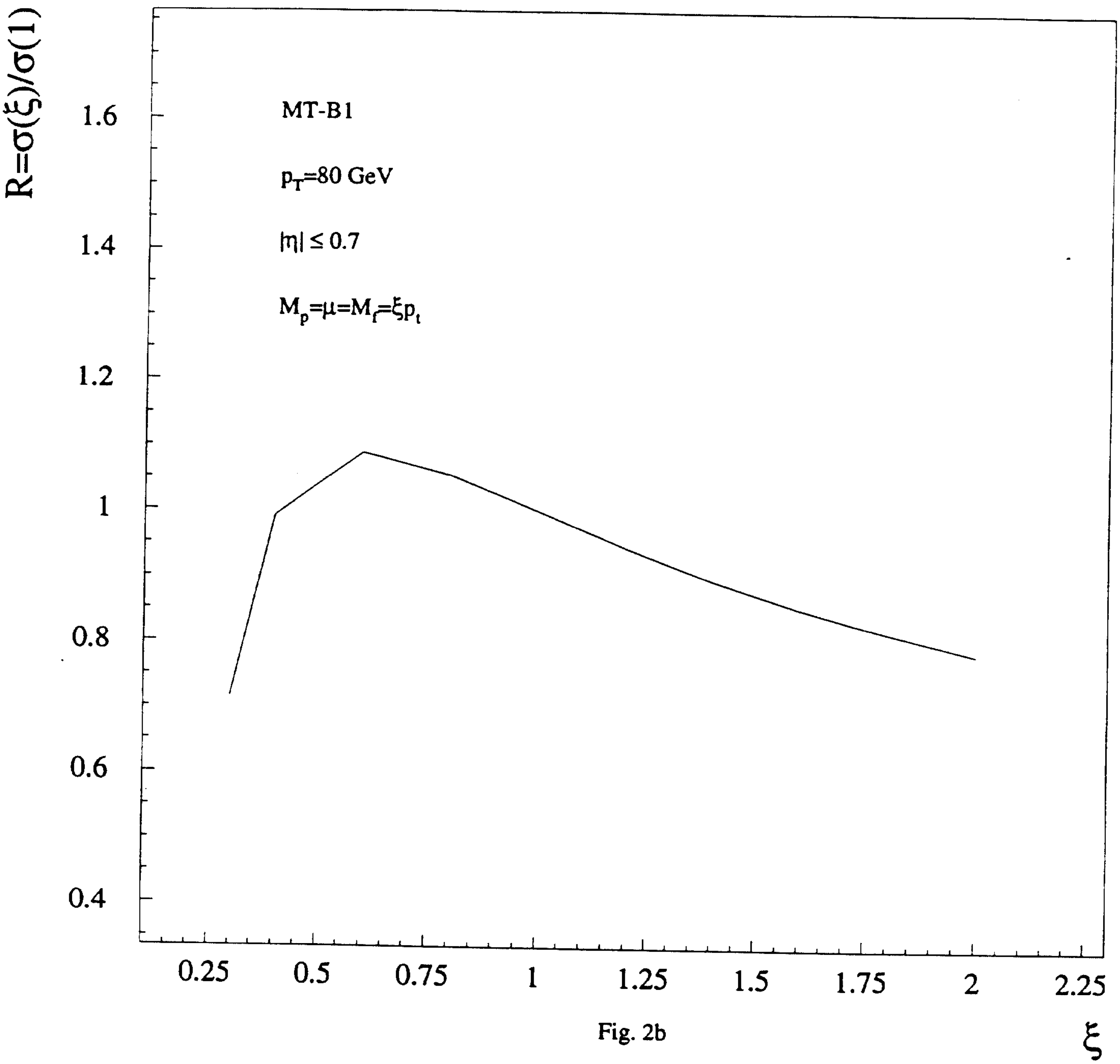

R=σ(ξ)/σ(1)
MT-B1
p_T=80 GeV
$|\eta| \leq 0.7$
$M_p=\mu=M_f=\xi p_t$
1.6
1.4
1.2
1
0.8
0.6
0.4
0.25
0.5
0.75
1
1.25
1.5
1.75
2
2.25
ξ

Fig. 2b

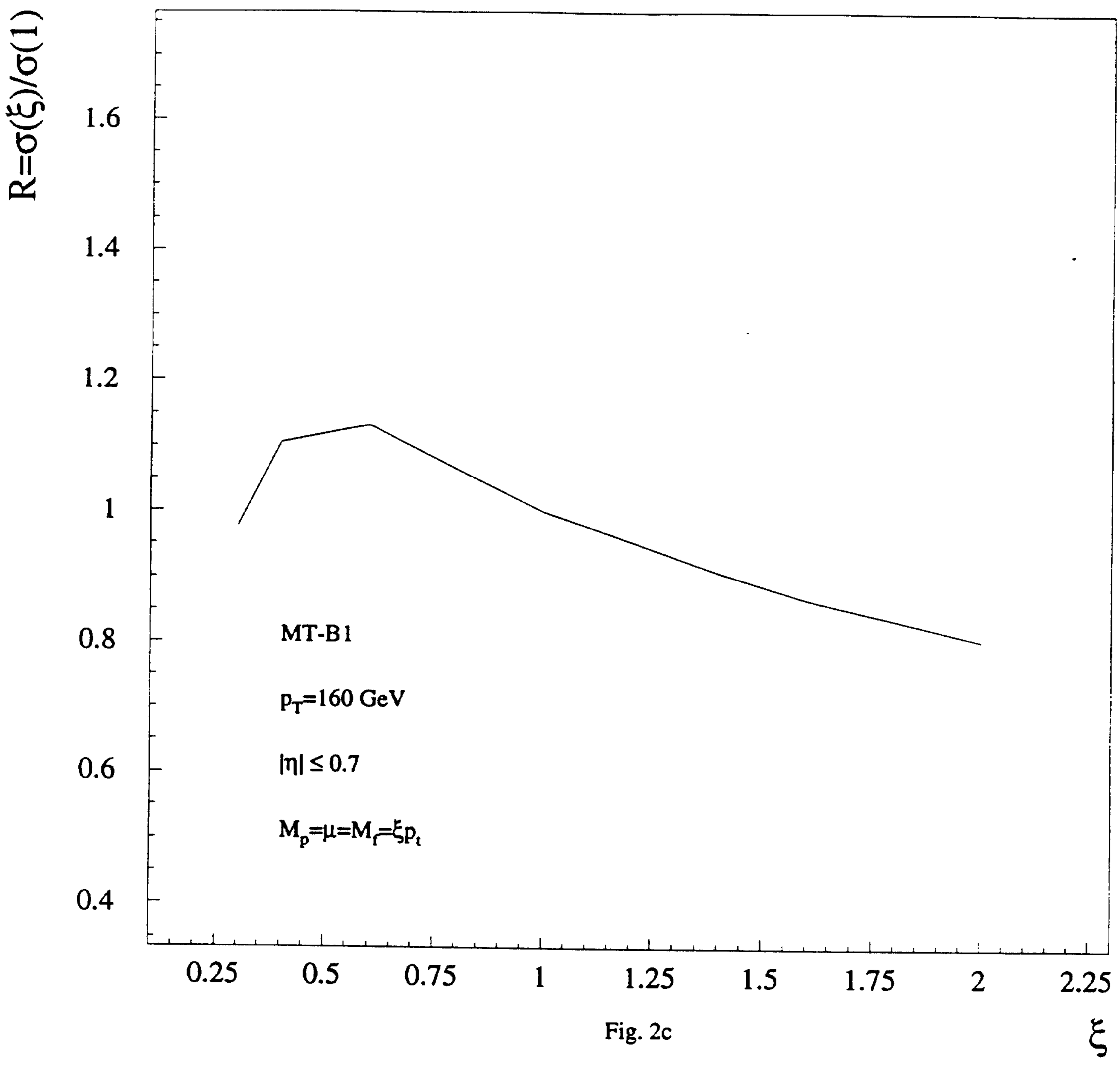
R=σ(ξ)/σ(1)
1.6
1.4
1.2
1
0.8
0.6
0.4
MT-B1
p_T=160 GeV
$|\eta| \leq 0.7$
$M_p=\mu=M_f=\xi p_t$
0.25
0.5
0.75
1
1.25
1.5
1.75
2
2.25
ξ

Fig. 2c

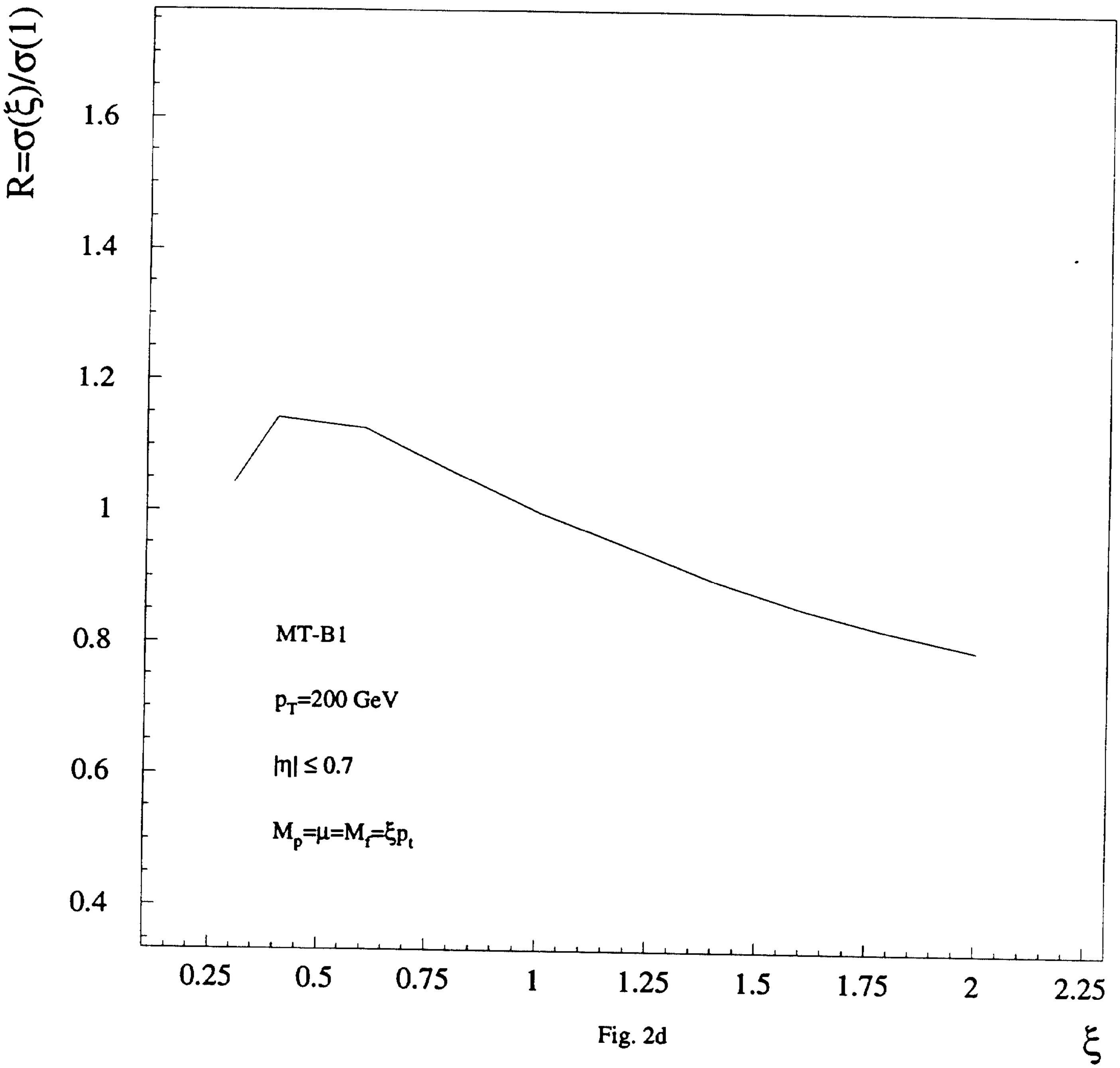

R=σ(ξ)/σ(1)
1.6
1.4
1.2
1
0.8
0.6
0.4
MT-B1
p_T=200 GeV
|η| ≤ 0.7
M_p=μ=M_f=ξp_t
0.25
0.5
0.75
1
1.25
1.5
1.75
2
2.25
ξ

Fig. 2d

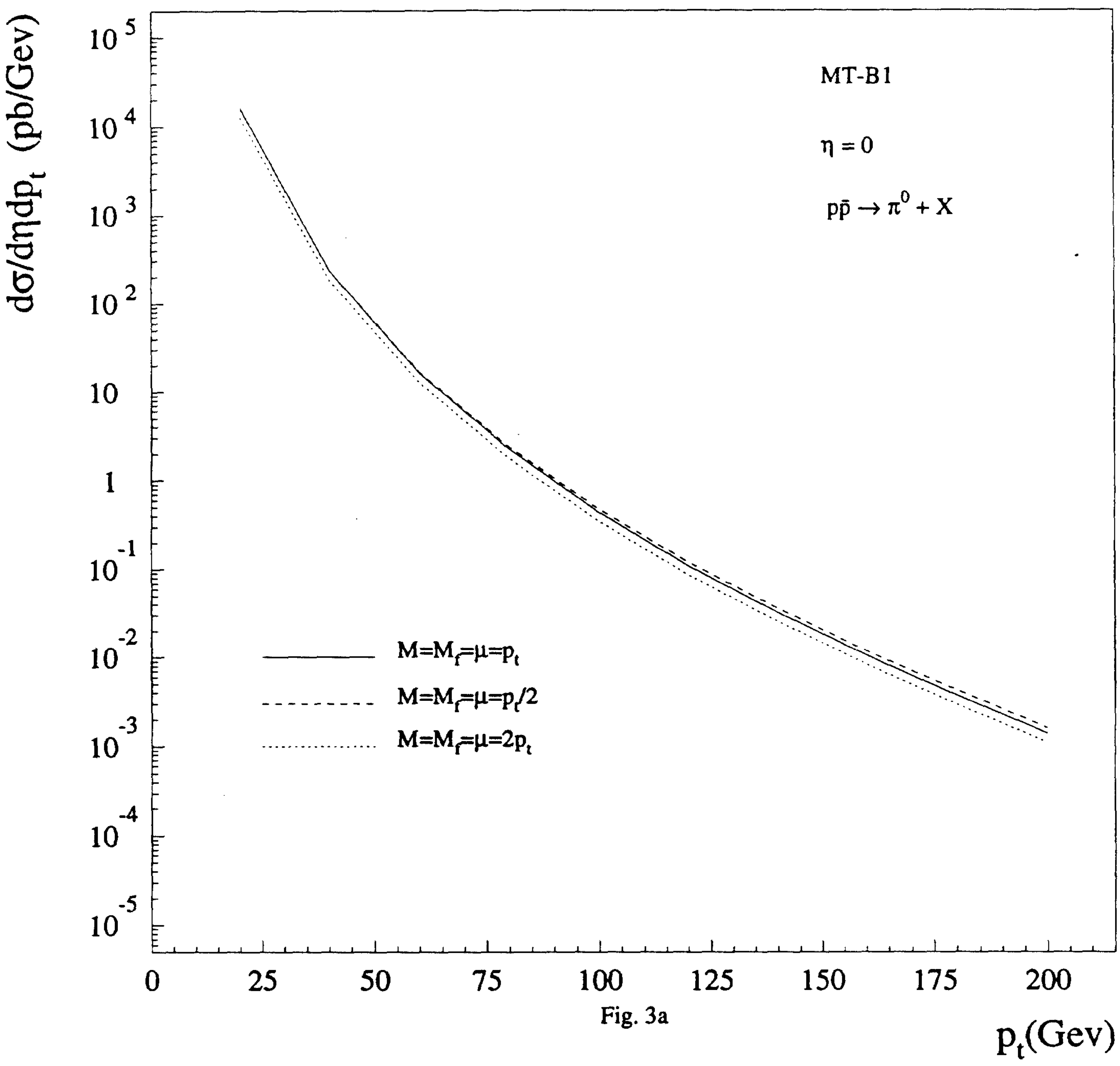

$d\sigma/d\eta dp_t$ (pb/Gev)
10^5
10^4
10^3
10^2
10
1
10^{-1}
10^{-2}
10^{-3}
10^{-4}
10^{-5}
MT-B1
$\eta = 0$
$p\bar{p} \rightarrow \pi^0 + X$
$M=M_f=\mu=p_t$
$M=M_f=\mu=p_t/2$
$M=M_f=\mu=2p_t$
0
25
50
75
100
125
150
175
200
p_t(Gev)

Fig. 3a

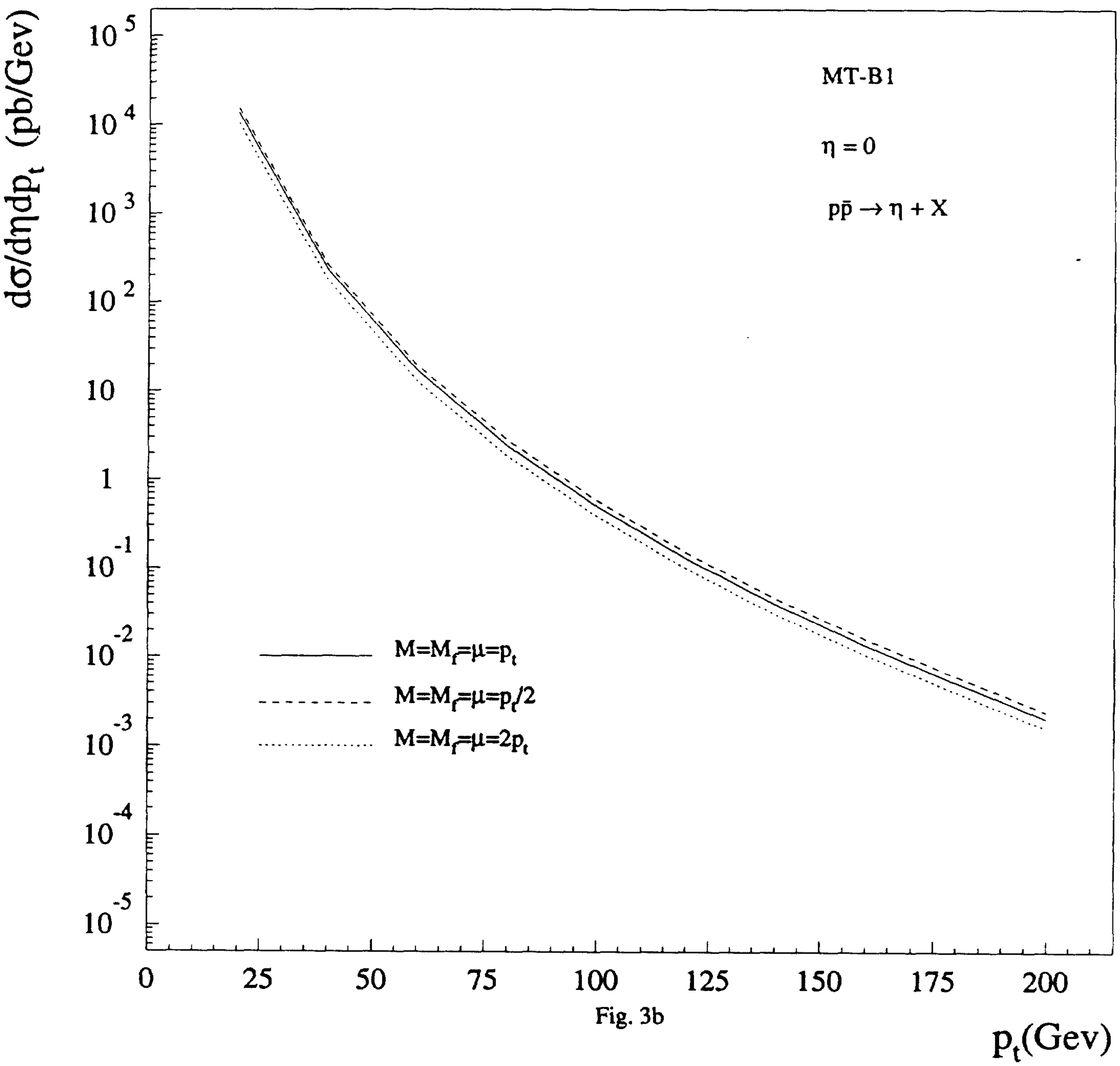

dσ/dηdp_t (pb/Gev)
10^5
10^4
10^3
10^2
10
1
10^-1
10^-2
10^-3
10^-4
10^-5
MT-B1
η = 0
pp̄ → η + X
M=M_f=μ=p_t
M=M_f=μ=p_t/2
M=M_f=μ=2p_t
0
25
50
75
100
125
150
175
200
p_t(Gev)

Fig. 3b

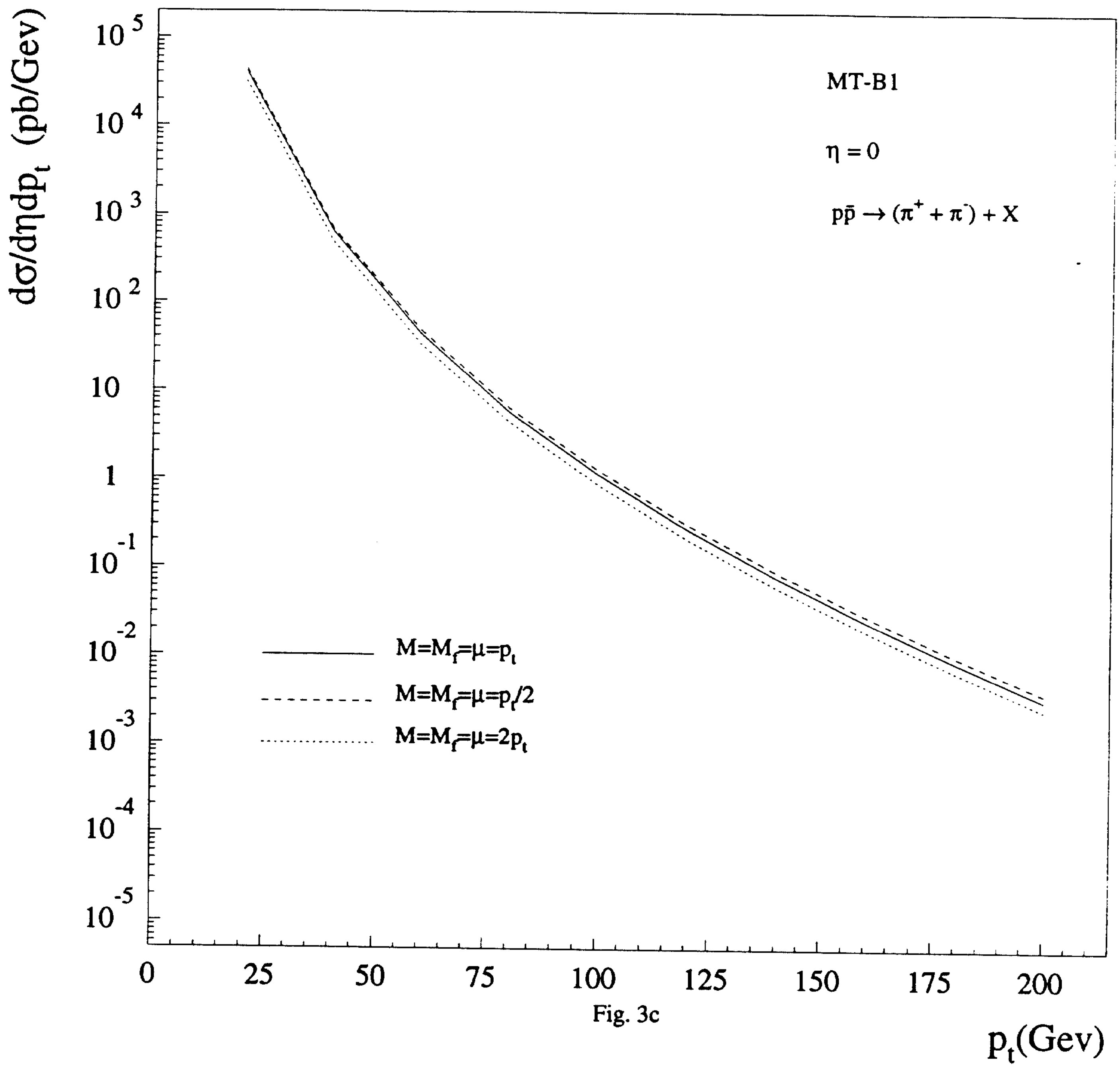

$d\sigma/d\eta dp_t$ (pb/Gev)
10^5
10^4
10^3
10^2
10
1
10^{-1}
10^{-2}
10^{-3}
10^{-4}
10^{-5}
0
25
50
75
100
125
150
175
200
MT-B1
$\eta = 0$
$p\bar{p} \rightarrow (\pi^+ + \pi^-) + X$
$M=M_f=\mu=p_t$
$M=M_f=\mu=p_t/2$
$M=M_f=\mu=2p_t$
p_t(Gev)

Fig. 3c

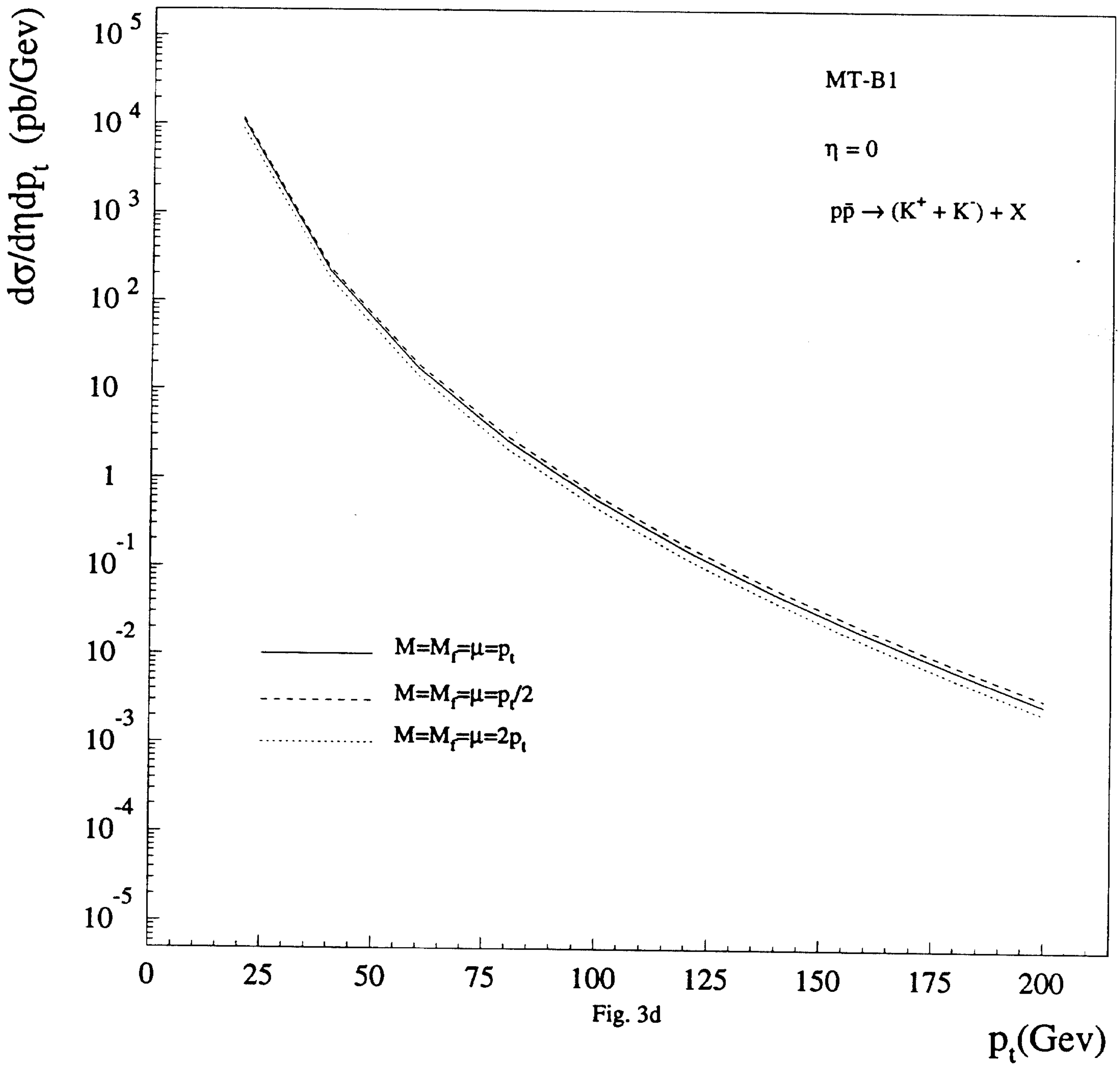

dσ/dηdp_t (pb/Gev)
10^5
10^4
10^3
10^2
10
1
10^-1
10^-2
10^-3
10^-4
10^-5
MT-B1
η = 0
pp̄ → (K⁺ + K⁻) + X
M=M_f=μ=p_t
M=M_f=μ=p_t/2
M=M_f=μ=2p_t
0
25
50
75
100
125
150
175
200
p_t(Gev)

Fig. 3d

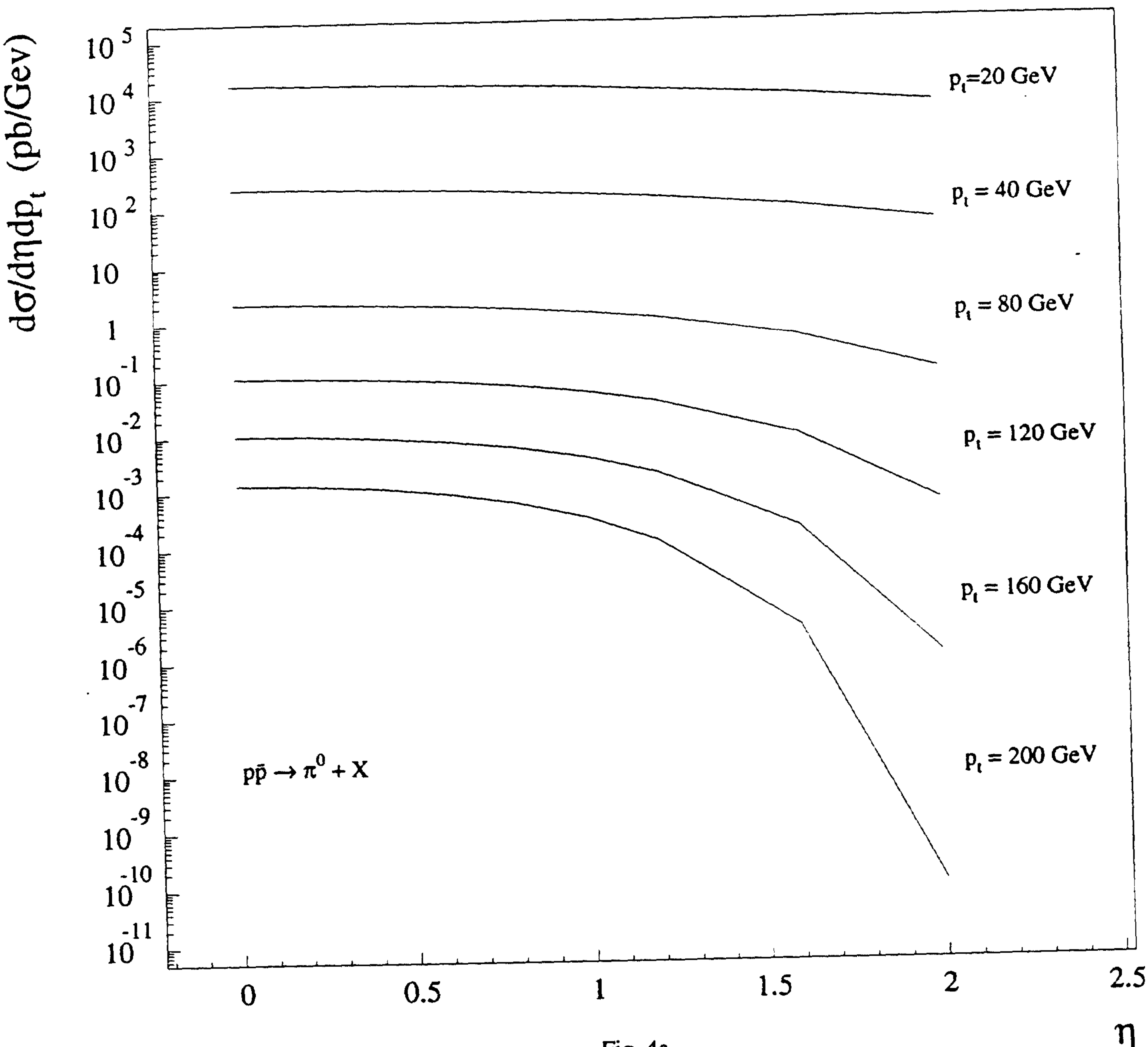

$d\sigma/d\eta dp_t$ (pb/Gev)
p_t=20 GeV
p_t = 40 GeV
p_t = 80 GeV
p_t = 120 GeV
p_t = 160 GeV
p_t = 200 GeV
$p\bar{p} \rightarrow \pi^0 + X$
η

Fig. 4a

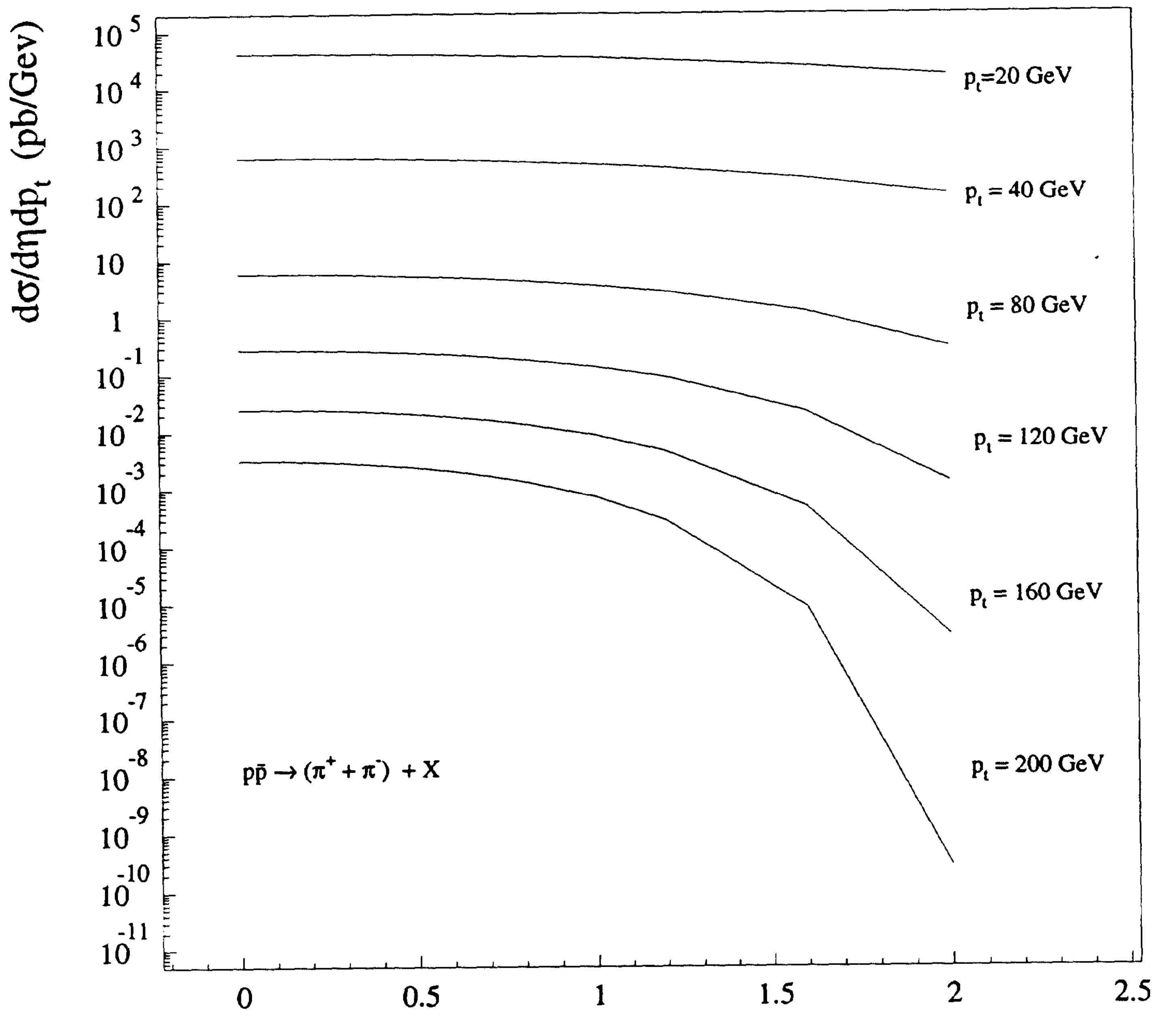

$d\sigma/d\eta dp_t$ (pb/Gev)
10^5
10^4
10^3
10^2
10
1
10^{-1}
10^{-2}
10^{-3}
10^{-4}
10^{-5}
10^{-6}
10^{-7}
10^{-8}
10^{-9}
10^{-10}
10^{-11}
p_t=20 GeV
p_t = 40 GeV
p_t = 80 GeV
p_t = 120 GeV
p_t = 160 GeV
p_t = 200 GeV
$p\bar{p} \rightarrow (\pi^+ + \pi^-) + X$
0
0.5
1
1.5
2
2.5
η

Fig. 4b

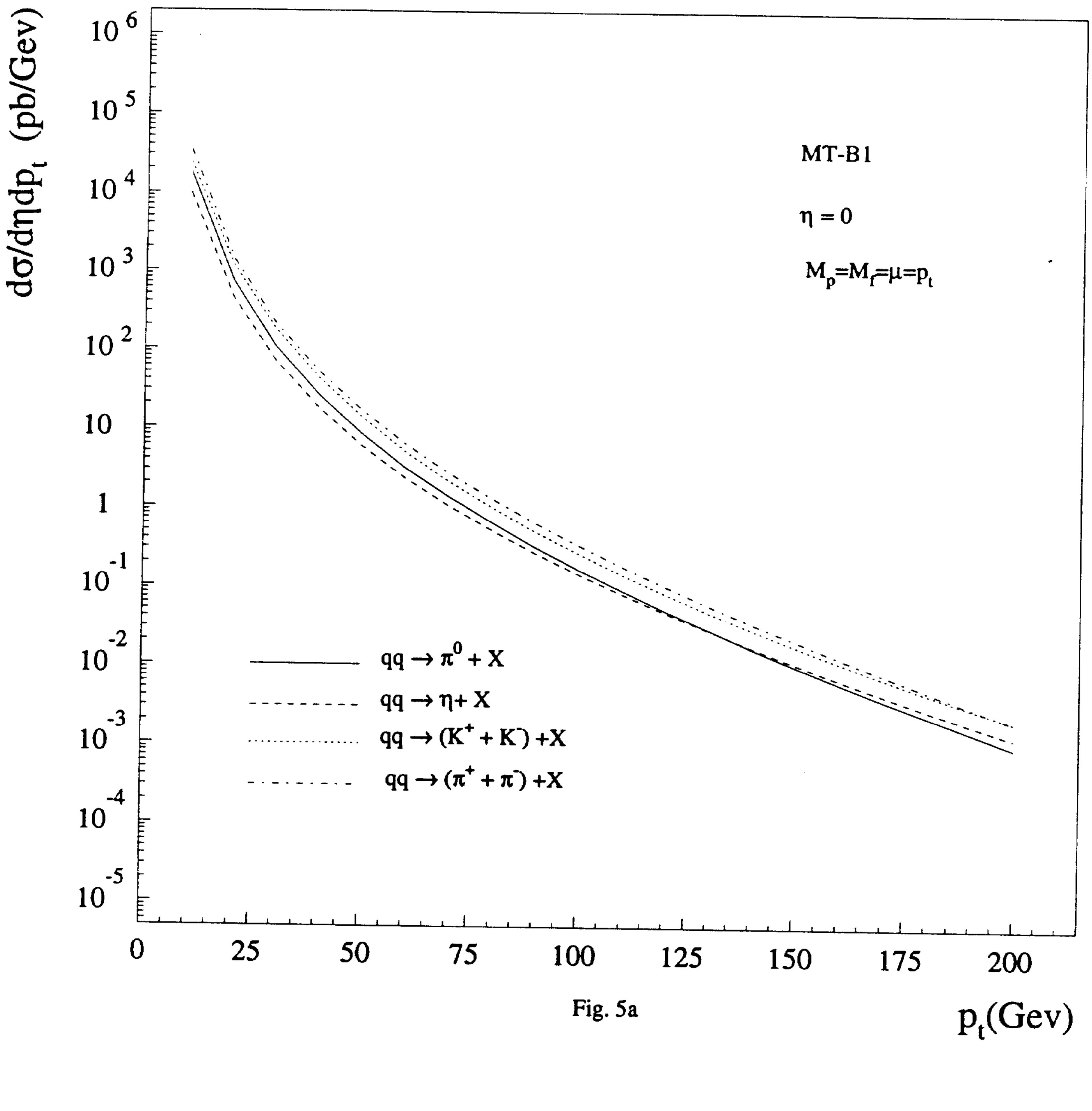

$d\sigma/d\eta dp_t$ (pb/Gev)
MT-B1
$\eta = 0$
$M_p=M_f=\mu=p_t$
$qq \to \pi^0 + X$
$qq \to \eta + X$
$qq \to (K^+ + K^-) + X$
$qq \to (\pi^+ + \pi^-) + X$
10^6
10^5
10^4
10^3
10^2
10
1
10^{-1}
10^{-2}
10^{-3}
10^{-4}
10^{-5}
0
25
50
75
100
125
150
175
200
p_t(Gev)

Fig. 5a

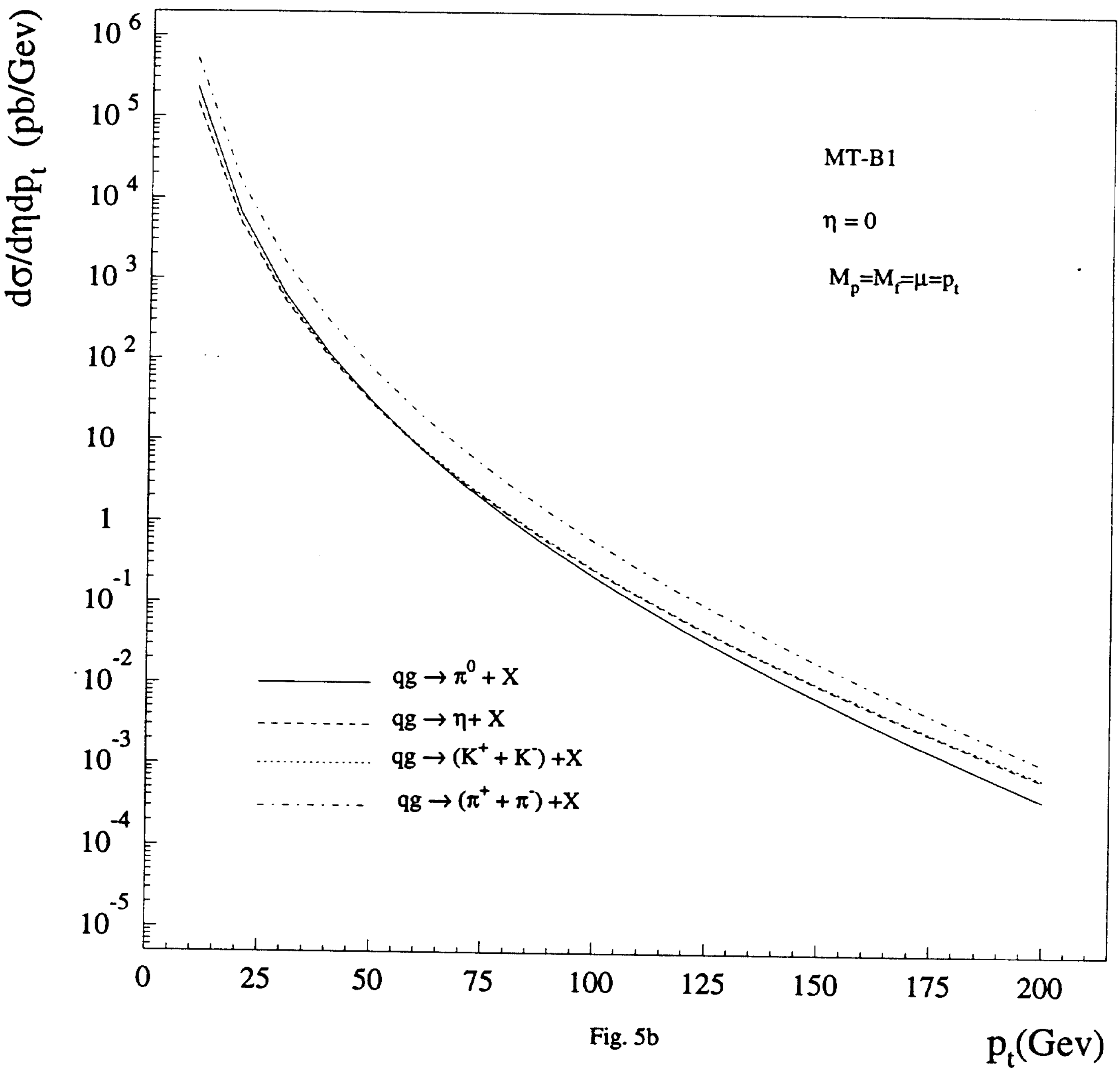

$d\sigma/d\eta dp_t$ (pb/Gev)
MT-B1
$\eta = 0$
$M_p=M_f=\mu=p_t$
$qg \to \pi^0 + X$
$qg \to \eta + X$
$qg \to (K^+ + K^-) + X$
$qg \to (\pi^+ + \pi^-) + X$
10^6
10^5
10^4
10^3
10^2
10
1
10^{-1}
10^{-2}
10^{-3}
10^{-4}
10^{-5}
0
25
50
75
100
125
150
175
200
p_t(Gev)

Fig. 5b

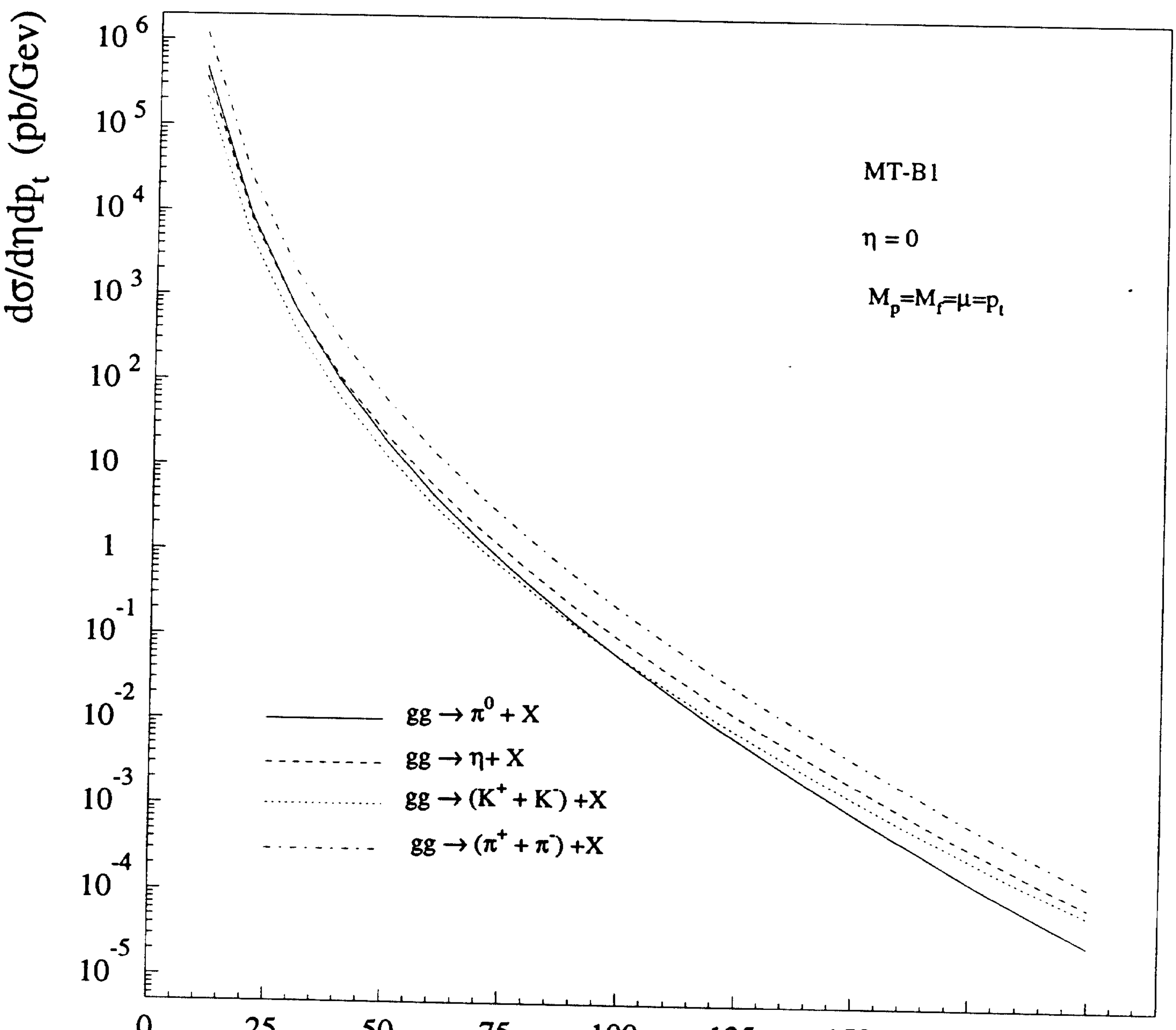
dσ/dηdp_t (pb/Gev)
MT-B1
η = 0
M_p=M_f=μ=p_t
gg → π^0 + X
gg → η+ X
gg → (K^+ + K^-) +X
gg → (π^+ + π^-) +X
p_t(Gev)
0
25
50
75
100
125
150
175
200
10^6
10^5
10^4
10^3
10^2
10
1
10^-1
10^-2
10^-3
10^-4
10^-5

Fig. 5c

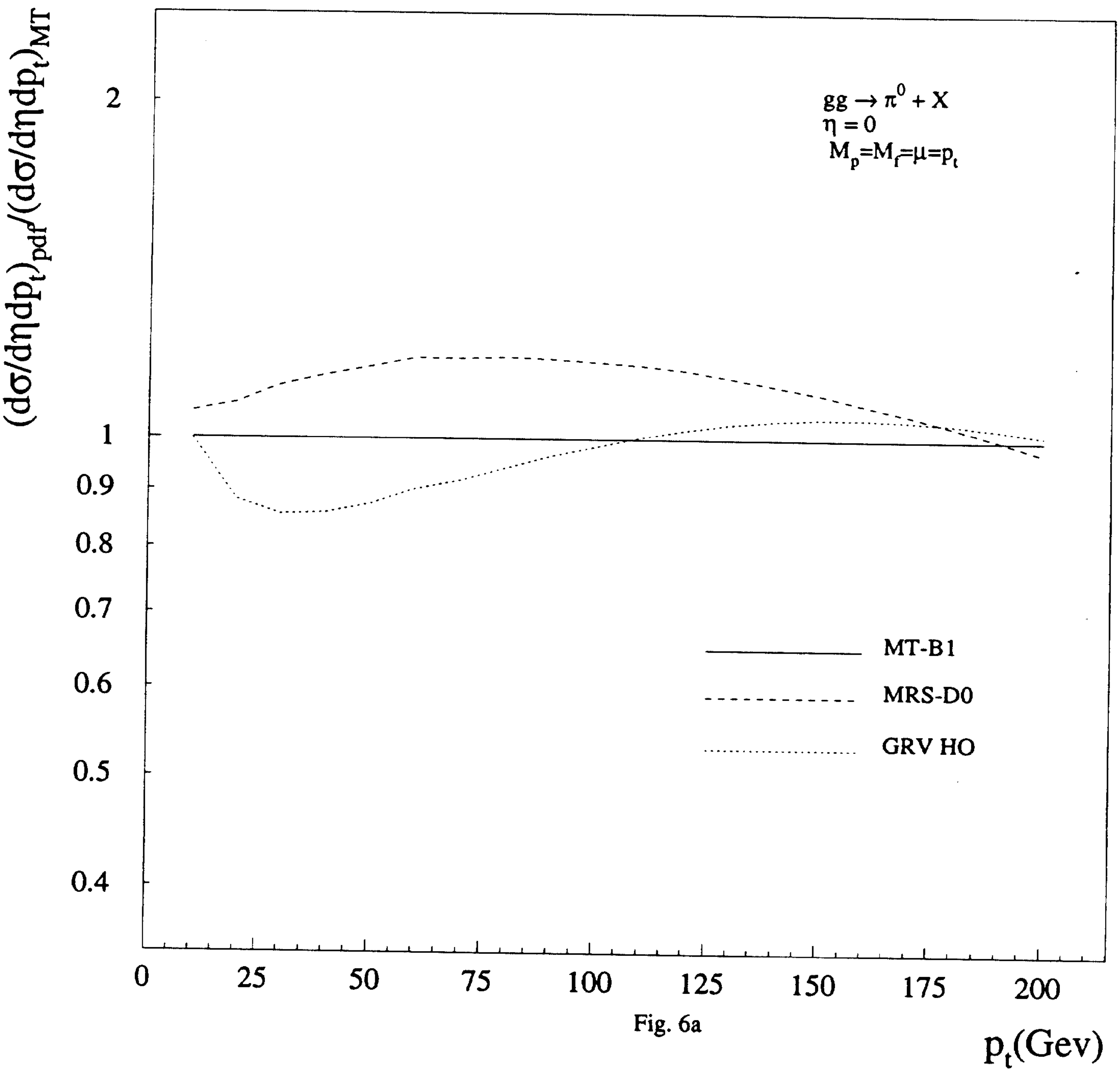
$(d\sigma/d\eta dp_t)_{pdf}/(d\sigma/d\eta dp_t)_{MT}$
2
1
0.9
0.8
0.7
0.6
0.5
0.4
$gg \rightarrow \pi^0 + X$
$\eta = 0$
$M_p=M_f=\mu=p_t$
MT-B1
MRS-D0
GRV HO
0
25
50
75
100
125
150
175
200
p_t(Gev)

Fig. 6a

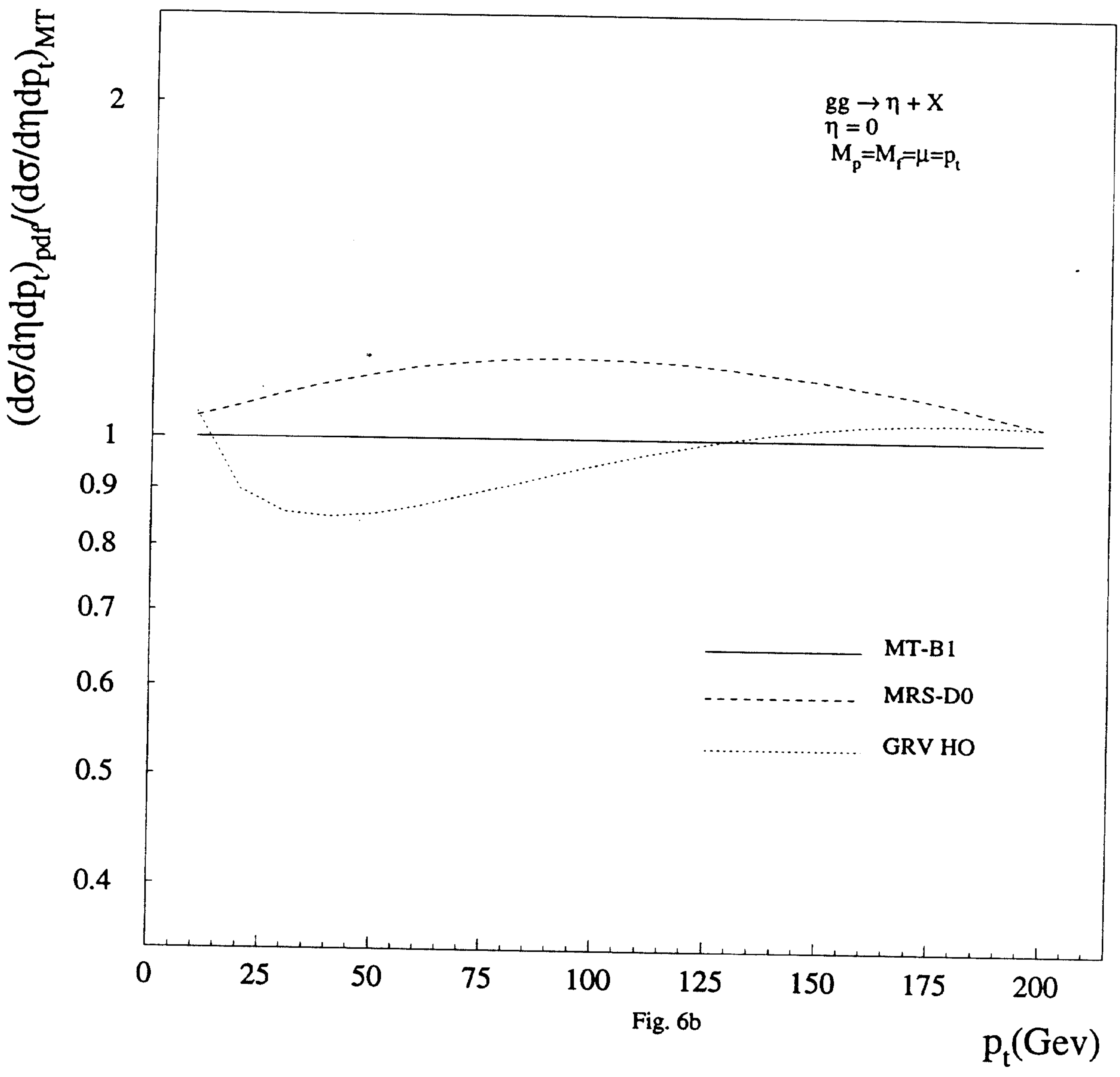

$(d\sigma/d\eta dp_t)_{pdf}/(d\sigma/d\eta dp_t)_{MT}$
2
1
0.9
0.8
0.7
0.6
0.5
0.4
0
25
50
75
100
125
150
175
200
$gg \to \eta + X$
$\eta = 0$
$M_p=M_f=\mu=p_t$
MT-B1
MRS-D0
GRV HO
p_t(Gev)

Fig. 6b

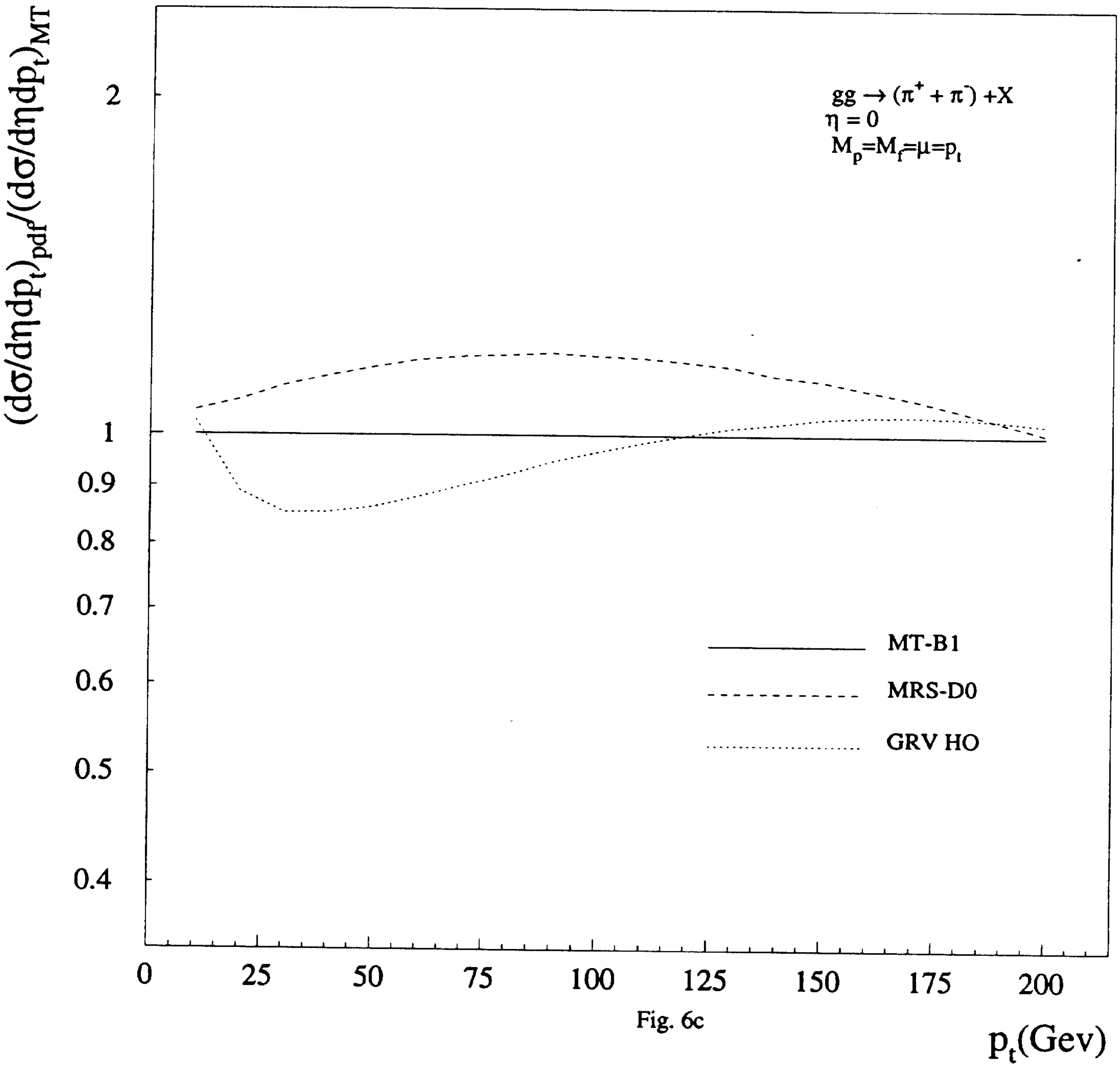

$(d\sigma/d\eta dp_t)_{pdf}/(d\sigma/d\eta dp_t)_{MT}$
2
1
0.9
0.8
0.7
0.6
0.5
0.4
$gg \to (\pi^+ + \pi^-) + X$
$\eta = 0$
$M_p = M_f = \mu = p_t$
MT-B1
MRS-D0
GRV HO
0
25
50
75
100
125
150
175
200
p_t(Gev)

Fig. 6c

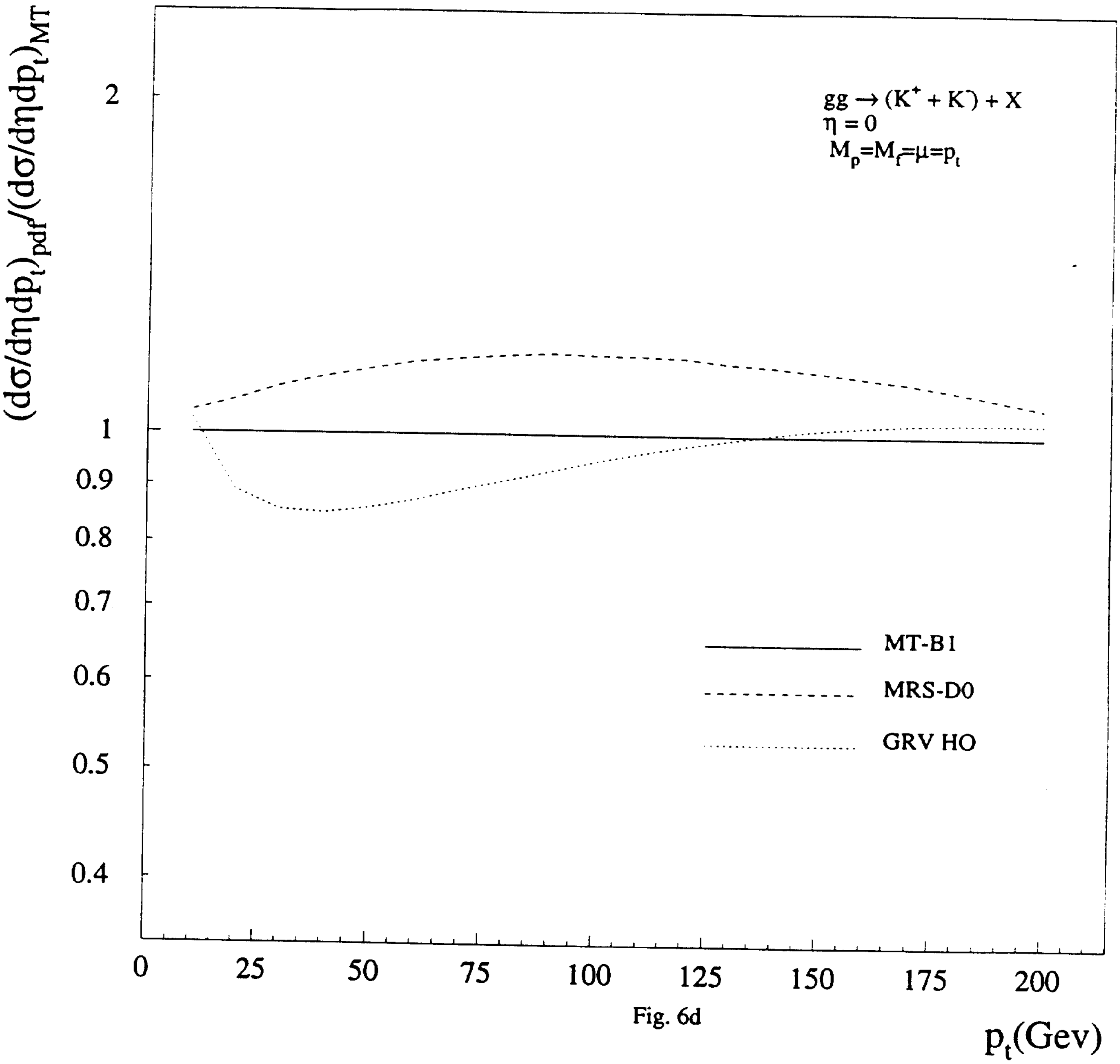
gg → (K⁺ + K⁻) + X
η = 0
Mp=Mf=μ=pt
MT-B1
MRS-D0
GRV HO
(dσ/dηdpt)pdf/(dσ/dηdpt)MT
2
1
0.9
0.8
0.7
0.6
0.5
0.4
0
25
50
75
100
125
150
175
200
pt(Gev)

Fig. 6d

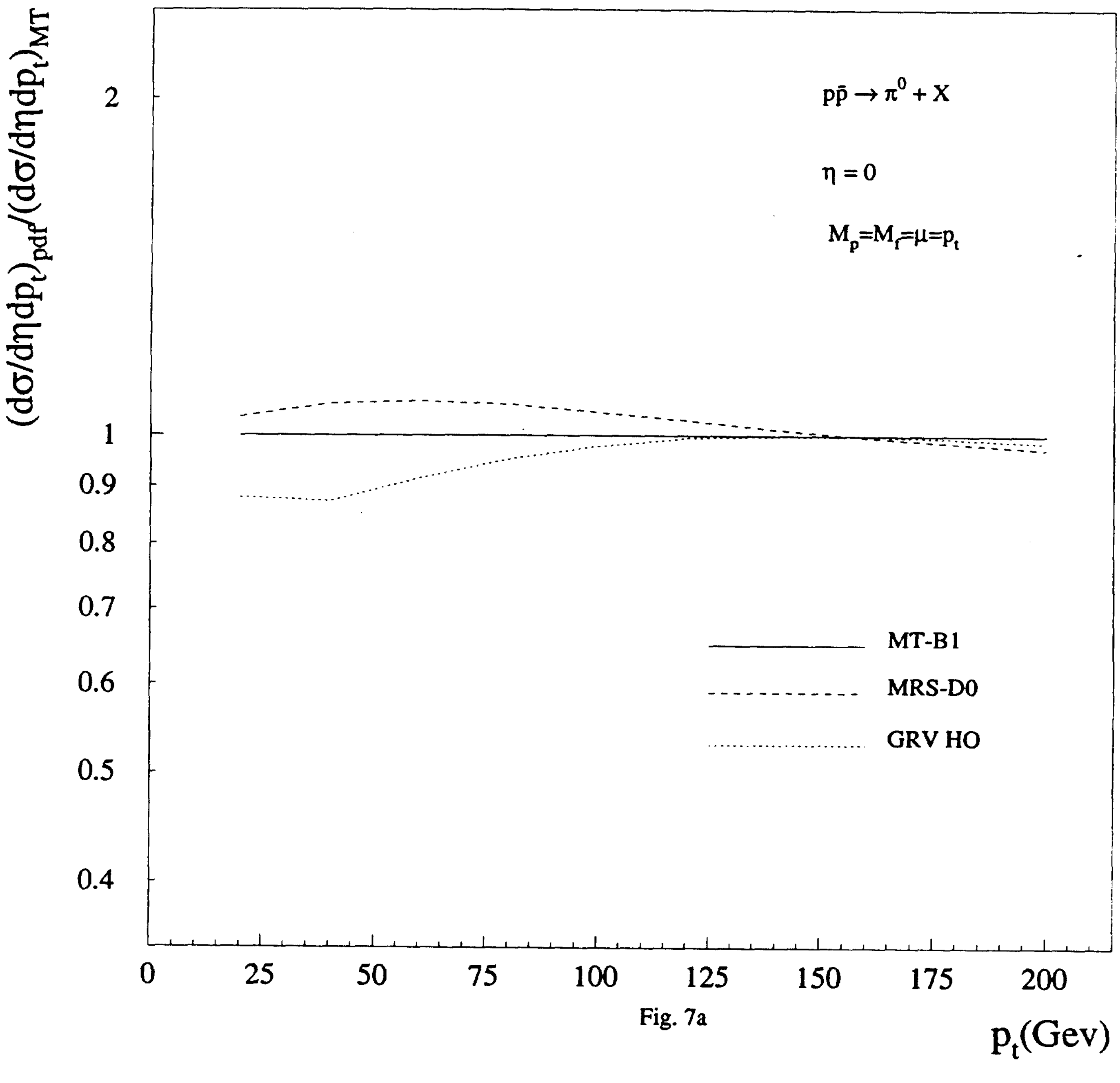

$(d\sigma/d\eta dp_t)_{pdf}/(d\sigma/d\eta dp_t)_{MT}$
2
1
0.9
0.8
0.7
0.6
0.5
0.4
$p\bar{p} \to \pi^0 + X$
$\eta = 0$
$M_p = M_f = \mu = p_t$
MT-B1
MRS-D0
GRV HO
0
25
50
75
100
125
150
175
200
p_t(Gev)

Fig. 7a

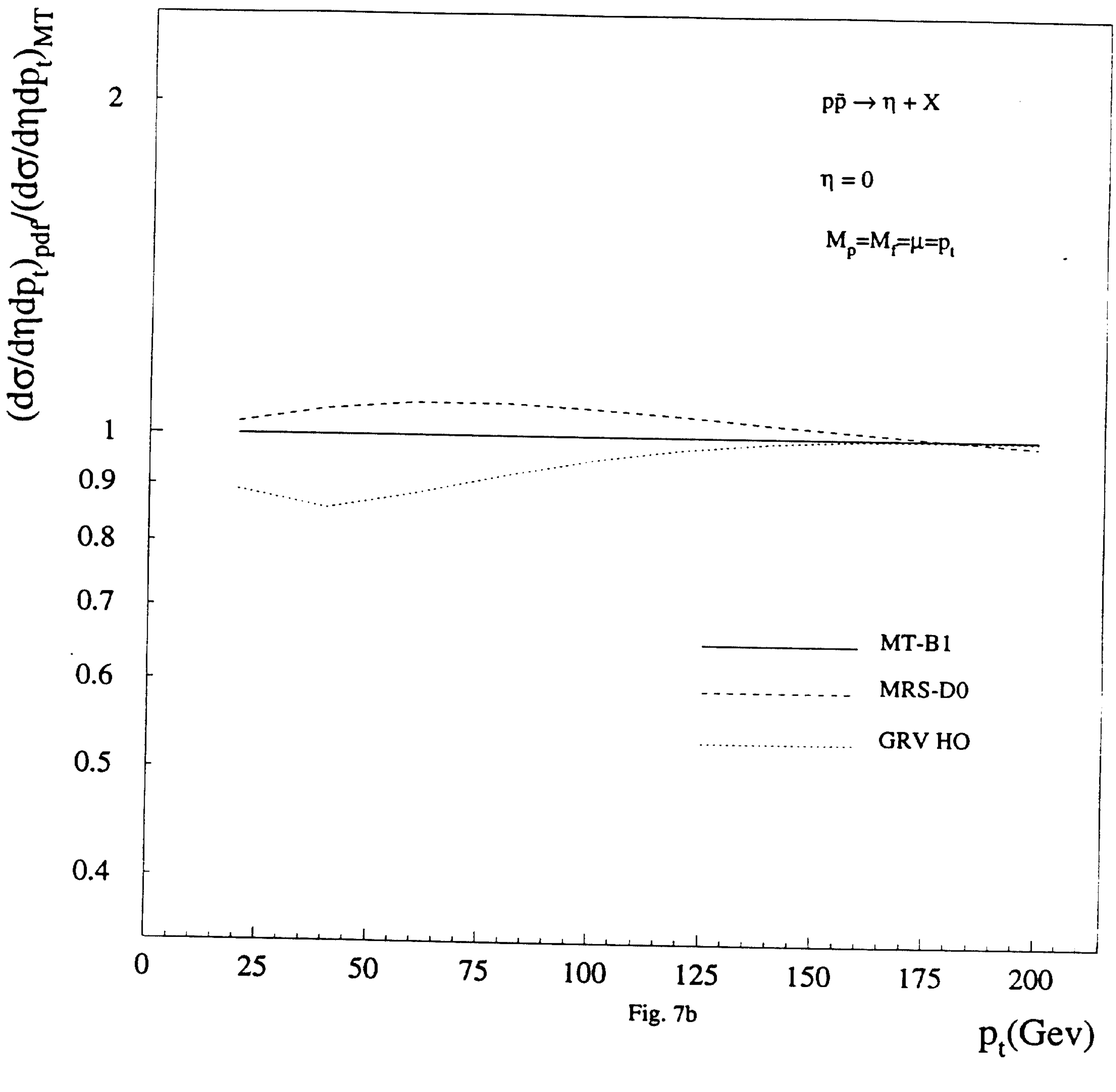
$(d\sigma/d\eta dp_t)_{pdf}/(d\sigma/d\eta dp_t)_{MT}$
2
1
0.9
0.8
0.7
0.6
0.5
0.4
0
25
50
75
100
125
150
175
200
$p\bar{p} \to \eta + X$
$\eta = 0$
$M_p=M_f=\mu=p_t$
MT-B1
MRS-D0
GRV HO
p_t(Gev)

Fig. 7b

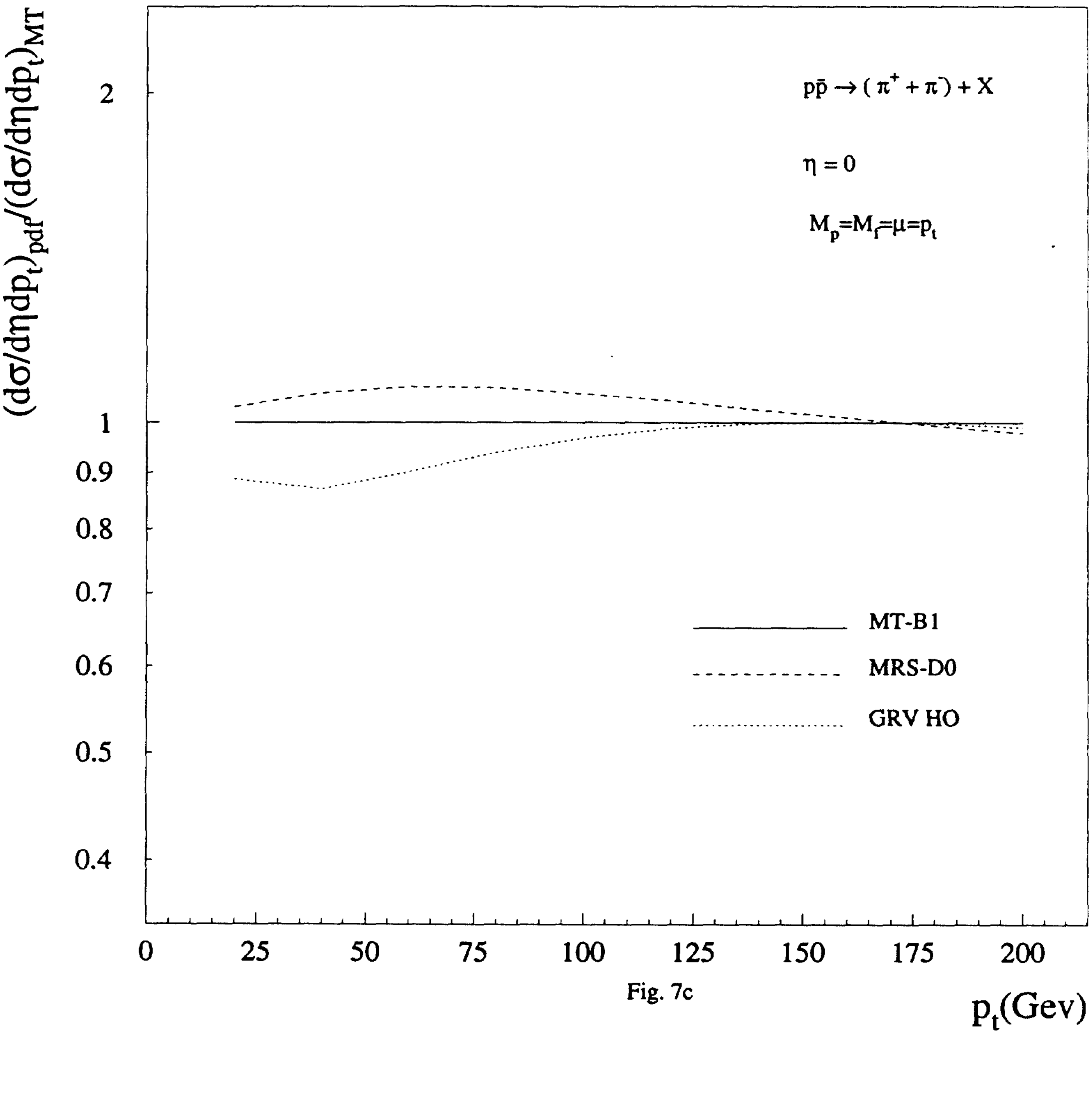

$(d\sigma/d\eta dp_t)_{pdf}/(d\sigma/d\eta dp_t)_{MT}$
2
1
0.9
0.8
0.7
0.6
0.5
0.4
$p\bar{p} \to (\pi^+ + \pi^-) + X$
$\eta = 0$
$M_p = M_f = \mu = p_t$
MT-B1
MRS-D0
GRV HO
0
25
50
75
100
125
150
175
200
p_t(Gev)

Fig. 7c

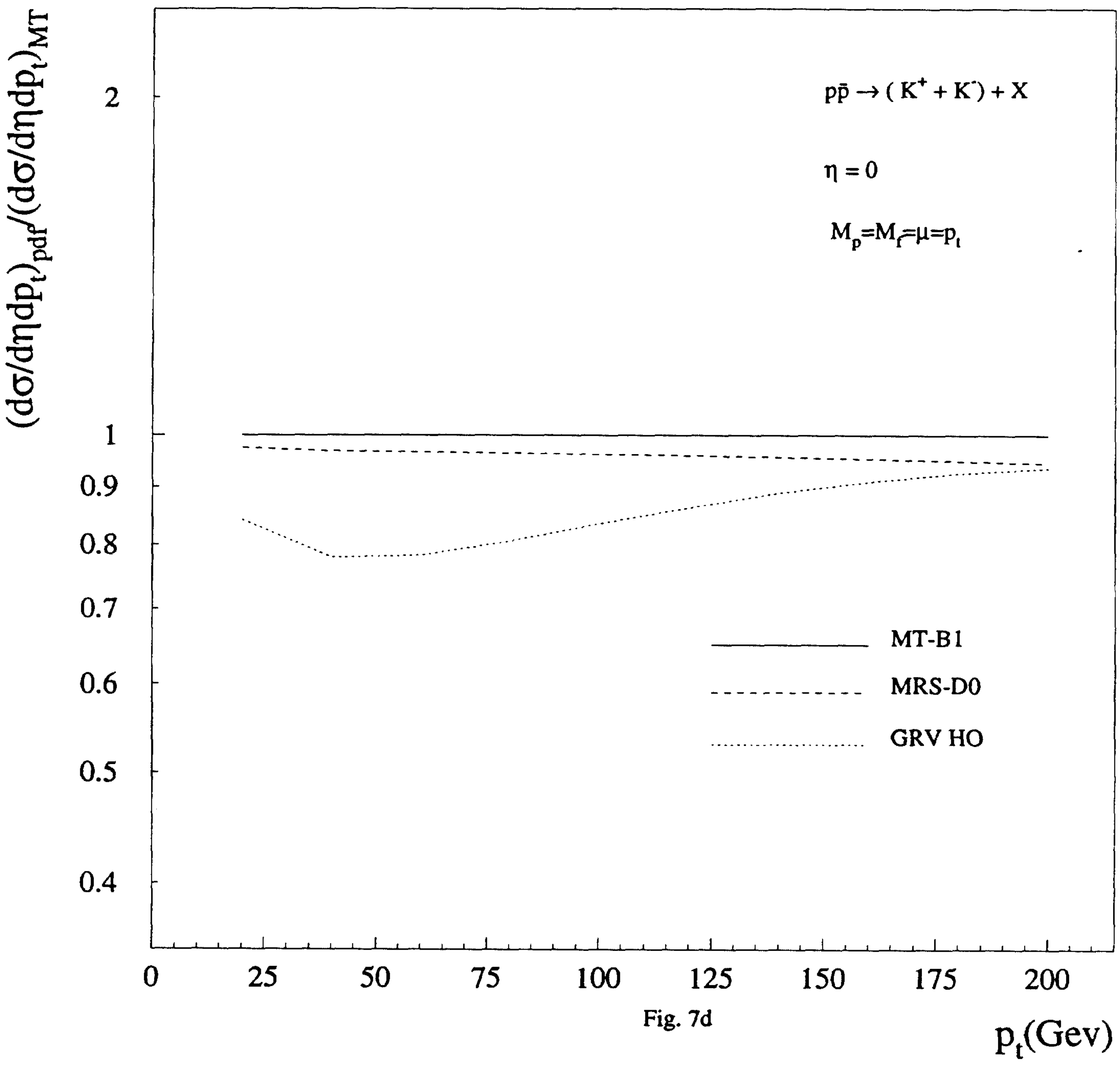
$(d\sigma/d\eta dp_t)_{pdf}/(d\sigma/d\eta dp_t)_{MT}$
$p\bar{p} \rightarrow (K^+ + K^-) + X$
$\eta = 0$
$M_p=M_f=\mu=p_t$
MT-B1
MRS-D0
GRV HO
2
1
0.9
0.8
0.7
0.6
0.5
0.4
0
25
50
75
100
125
150
175
200
p_t(Gev)

Fig. 7d

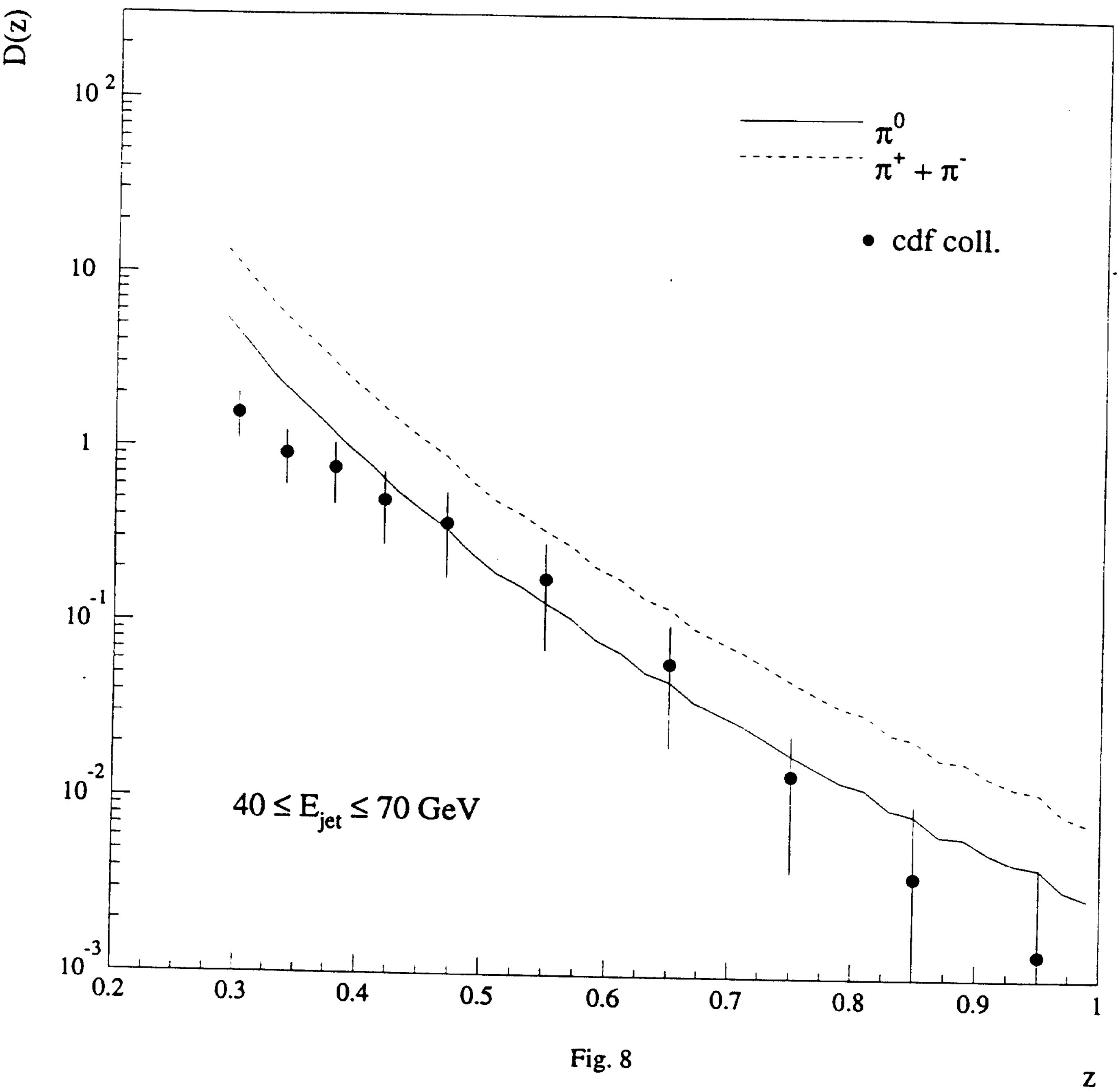
D(z)
10^2
10
1
10^{-1}
10^{-2}
10^{-3}
π^0
$\pi^+ + \pi^-$
cdf coll.
$40 \leq E_{jet} \leq 70$ GeV
0.2
0.3
0.4
0.5
0.6
0.7
0.8
0.9
1
z

Fig. 8